NACA

RESEARCH MEMORANDUM

PREFLIGHT TESTS AND FLIGHT PERFORMANCE OF A

6.5-INCH-DIAMETER RAM-JET ENGINE

By Arthur H. Hinners, Jr., and Douglas H. Foland

Langley Aeronautical Laboratory
Langley Field, Va.

NATIONAL ADVISORY COMMITTEE
FOR AERONAUTICS

WASHINGTON

November 2, 1953

Classification cancelled (or changed to Unclassified)

By Authority of Mgt. Tech. Assignment #3
(OFFICER AUTHORIZED TO CHANGE)

By ..... 4 Feb 57
NAME AND

..... USAF
GRADE OF OFFICER MAKING CHANGE)

4 Feb 57
DATE

NATIONAL ADVISORY COMMITTEE FOR AERONAUTICS

RESEARCH MEMORANDUM

PREFLIGHT TESTS AND FLIGHT PERFORMANCE OF A 6.5-INCH-DIAMETER RAM-JET ENGINE

By Arthur H. Hinners, Jr., and Douglas H. Foland

SUMMARY

A 20° semiangle conical-inlet ram-jet engine having a design Mach number of 2.13 was tested in free supersonic jets at Mach numbers of 1.84, 2.06, and 2.21 to determine its inlet and combustion performance over a fuel-air ratio range of approximately 0.010 to 0.087. Comparisons are made with inlet cold-flow tests at Mach numbers of 2.00 and 2.25.

A flight investigation of this same engine was made by using a supersonic twin-engine ram-jet test vehicle. Ram-jet performance data were obtained over a Mach number range of 1.76 to 2.61 and an altitude range from 1,400 to 63,600 feet using ethylene (C_2H_4) as a fuel. Although the ram jet buzzed from a Mach number of 1.76 to 1.85, the engine was able to sustain combustion and the engine thrust was sufficient to accelerate the model. A maximum gross thrust coefficient of 0.78 was reached at a free-stream Mach number of 2.36. Ram-jet burnout occurred at a Mach number of 2.48. After burnout the vehicle coasted to a peak altitude of 105,000 feet.

Maximum total-pressure recoveries of 0.88, 0.80, and 0.77 were obtained at free-jet Mach numbers of 1.84, 2.06, and 2.21, respectively, in preflight combustion performance tests. Maximum total-pressure recoveries of 0.85 and 0.78 were obtained at free-jet Mach numbers of 2.00 and 2.25, respectively, in cold-flow tests. Maximum thrust coefficients of 0.77, 0.87, and 0.91 were attained at free-jet Mach numbers of 1.84, 2.06, and 2.21, respectively. Maximum values of air impulse efficiency and combustion efficiency were 96 percent and 84 percent, respectively, near a fuel-air ratio of 0.03. The lowest value of specific fuel consumption was 2.4 at a Mach number of 2.06.

Increases in thrust coefficient of 20.3 percent and 6.2 percent at fuel-air ratios of 0.06 and 0.08, respectively, were found at a test Mach number of 2.00 over values of thrust coefficient attained with an engine of identical design except for a 25-percent smaller capture area.

[redacted]

INTRODUCTION

Test results of a 20° semiangle central-body-type ram-jet engine were reported in references 1 and 2. A modification of this engine in which the capture area was increased by approximately 25 percent to improve the thrust performance at the design Mach number has been flight-tested as a twin-engine ram-jet test vehicle and was reported in reference 3. This model was launched at an elevation angle of 75°, and flown along a zero-lift trajectory.

Another twin-engine ram-jet vehicle has been flown along a zero-lift trajectory from a launching angle of 60°. The engines of the present test were similar to the engines of reference 3 except that the exit nozzle contraction ratio was 8 percent smaller. The results of this test are presented in this paper.

In order to obtain more detailed information about the performance of this modified engine, cold-flow and combustion free-jet tests were made in the preflight jet of the Langley Pilotless Aircraft Research Station at Wallops Island, Va. The results of these tests at 0° angle of attack and 0° angle of yaw are also presented in this paper.

SYMBOLS

A	cross-sectional area of duct, sq ft
A_{cowl}	projected inlet frontal area, sq ft
A_e	entrance area to diffuser defined along surface perpendicular to cone surface from cowling lip, sq ft
C_c	combustor-force coefficient, based on combustion-chamber area (0.231 sq ft), $C_c = \frac{G}{H_5 A_8}$
C_D	drag coefficient
$(C_p)_c$	specific heat of products of combustion at constant pressure, Btu/lb °R
$(\bar{C}_p)_c$	mean specific heat of products of combustion at constant pressure, Btu/lb °R

$(C_P)_m$	specific heat of fuel-air mixture at constant pressure, Btu/lb $^{\circ}R$
$(\bar{C}_P)_m$	mean specific heat of fuel-air mixture at constant pressure, Btu/lb $^{\circ}R$
C_T	thrust coefficient, based on combustion-chamber area
D	drag, lb
D_t	tare drag, lb
d	diameter, in.
F	engine thrust, lb
f/a	fuel-air ratio, weight rate of fuel flow to weight rate of air flow
g	acceleration due to gravity, 32.2 ft/sec^2
G	actual jet propulsive force, lb
G'	ideal jet propulsive force, lb
H	total pressure, lb/ft^2 abs
Δh	heat release for ethylene as a function of the temperature rise, Btu
h_c	lower heating value of ethylene, 20,400 Btu/lb fuel
J	mechanical equivalent of heat, 778 ft-lb/Btu
M	Mach number
m	measured air mass flow through duct, slugs/sec
m_0	air mass flow through a stream tube of area equal to the inlet capture area at free-stream conditions, slugs/sec
P	static pressure, lb/ft^2 abs
R	universal gas constant, 53.3 $ft/^{\circ}R$
R_e	Reynolds number, based on cowl lip diameter

r	radius of duct at measuring station, in.
S_a	air specific impulse, sec
S_a'	ideal air specific impulse, sec
S_f	fuel specific impulse, sec
T	free-stream static temperature, $^{\circ}R$
T_a	static temperature of products of combustion, $^{\circ}R$
$(T_s)_a$	total temperature of products of combustion, $^{\circ}R$
$(T_s)_b$	total temperature of fuel-air mixture entering combustion chamber, $^{\circ}R$
V	velocity, ft/sec
W_a	weight flow of air, lb/sec
W_f	weight flow of fuel, lb/sec
x	distance from cone tip (positive downstream), in.
X	force measured on thrust stand, lb
y	ordinate of total-pressure tube measured radially from center line of model, in.
γ	ratio of specific heats, $\gamma = 1.4$
γ_a	ratio of specific heats of products of combustion
η_c	combustion efficiency, $\frac{\Delta h}{W_f h_c}$
η_i	air impulse efficiency, $\frac{G_{10}}{G_{10}'}$
ρ	density, slugs/sec
$\phi(M)$	ratio of jet impulse at any station to the jet impulse at a sonic station

Subscripts:

0	free stream
1	a point station behind conical shock
2	cone surface
3	station of minimum internal area or diffuser throat, 0.0677 sq ft
4	combustion rake station, 0.1533 sq ft, or cold-flow rake station, 0.1520 sq ft
5	diffuser exit station, combustion performance model, 0.1844 sq ft, or cold-flow model, 0.1921 sq ft
6	cold-flow choking station, $M_6 = 1.00$
7	cold-flow simulated combustion exit station, 0.1892 sq ft
8	combustion performance model static pressure station, 0.2310 sq ft
9	combustion performance model nozzle throat, 0.1964 sq ft
10	cold-flow exit choking station and combustion performance model nozzle exit
l	local point station
SL	sea-level standard condition

MODELS

Preflight Tests

Three photographs of the ram-jet engine and a sketch of the models tested are presented as figures 1 and 2, respectively. The overall length of the ram-jet engine with combustion chamber was 50.69 inches, with a maximum diameter of 6.60 inches. The conical inlet utilized a 20° semiangle cone which projected 3.02 inches forward of the inlet lip. The Mach number at which the oblique shock from the innerbody cone tip intersects the cowl lip is commonly called the design Mach number of the inlet, which for the subject engine was 2.13. The contraction ratio A_e/A_3

was 1.16. Coordinates of the central body and the inlet cowl are given in table I. The ratio of the central-body maximum diameter to the cowl-lip diameter is 0.68.

The innerbody was supported and centered in the inlet cowl by two diametrically opposite circular-arc struts. Fuel lines passed through one of the support struts to transport fuel from outside the model to inside the innerbody and from there to the burner which attached to the after end of the innerbody. The fuel-cooled "donut" burner, fuel-spray assembly, and combustor shell were all constructed of Inconel and are more completely described in reference 2.

For cold-flow tare drag tests, the donut burner of the combustion model was replaced with a rod which supported a tail plug (fig. 2(b)), which fixed the outlet area for each test. Appropriate plug diameters were selected to give variations in diffuser back pressure.

For cold-flow tests a variable-exit-area attachment shown in figure 2(c) was used to regulate the mass flow. Rakes and static orifices were installed as shown.

The station notation used in data presentation and analysis is shown in figure 3.

Flight-Test Vehicle and Engines

The flight-test vehicle with twin-ram-jet engines installed on the tail surfaces and the double-rocket booster are shown on the zero-length launching rack in figure 1(d).

The principal dimensions and general arrangement of the test vehicle are shown in figure 2(d). The vehicle was 15 feet $9\frac{1}{2}$ inches long and weighed $242\frac{1}{2}$ pounds including 22 pounds of fuel.

The two ram-jet engines which were mounted on the horizontal tail surfaces were the same as the ground-test engine previously described, with the exception that the overall length was 47.20 inches long due to a shorter combustion chamber and the exit nozzle was $5\frac{3}{4}$ inches in diameter rather than 6 inches in diameter. The exit-nozzle contraction ratio was therefore 0.785 and the expansion ratio, 0.760.

Ignition of the engines was accomplished by means of a starting disk and two electric delay squibs in each engine after take-off. The fuel used was ethylene (C_2H_4) and the fuel system was similar to that used in the model of reference 3. The fuel flow was to be regulated by an

electrically operated valve, but the regulator failed to function. As a result the valve opened to the full-opened position shortly after ignition and remained open during the entire flight.

INSTRUMENTATION AND MEASUREMENTS

Preflight Tests

Total pressure at the diffuser exit station (station 5) in the cold-flow model was determined by 19 total-pressure tubes located across the diameter, perpendicular to the innerbody support struts. The static pressure was determined by two wall static orifices and two rake static probes. A small rake at station 4 consisted of six total-pressure tubes, one wall static orifice, and one static probe. This rake was located at 45° from the plane of the innerbody support struts. Twelve static orifices were located on the model innerbody, equally spaced from a position of $\frac{x}{d_5} = 0.446$ to $\frac{x}{d_5} = 1.135$ $\left(\frac{x}{d_5} = 0 \text{ at cone tip}\right)$.

The combustion model had a manifolded rake at station 4. The five tubes of this rake were spaced at radial stations of equal area, and were all connected to a common pressure chamber within the rake. This chamber pressure was measured to obtain an approximate average total pressure. These tubes were individually measured during tests at $M_0 = 2.21$ to determine the Mach number profile. Static-pressure orifices were located at stations 4, 5, and 8.

During tare-drag tests, the engine was mounted on a force balance and instrumentation was installed to determine the internal drag. Two manifolded rakes were located at station 7. Two rakes were located radially 90° apart and 45° from the plane of the inner-body support struts. The measured chamber pressures of the two rakes were arithmetically averaged to obtain average total pressure at this station. A static orifice was also located at this station. A static-pressure orifice in the tail plug allowed measurement of the base pressure.

Thrust measurements were made with a strain-gage beam balance. Measurements of the fuel-flow pressures and fuel temperatures were obtained with electrical pressure pickups and thermocouples. Other measurements made were: the free-stream total pressure in the settling chamber just before the free-jet supersonic nozzle, the free-jet stagnation temperature, and the stream static pressures along a wall parallel to the axis of of the free-jet nozzle. All pressures were measured and recorded by either mechanical-optical pressure recorders or electrical pressure pickups of the strain-gage type with oscillograph recorders. Time histories

were obtained on film and paper records which were time-correlated by a 10-cycle-per-second timer. Observations of the flow were made by a shadowgraph system and were photographed at an exposure of approximately 0.003 second.

The free-jet supersonic nozzles were calibrated from static-pressure measurements along the nozzle wall from the throat to the nozzle exit, from total-pressure measurements of the flow at and near the nozzle exit, and from measurements of the oblique-shock angles in shadowgraph pictures of the free-jet flow over cones.

Flight Test

An NACA 10-channel telemeter measured free-stream pitot stagnation pressure, free-stream static pressure (at a point on the body 12 diameters from the base of the conical nose), longitudinal acceleration, the setting of a linear-control-position indicator (fuel-control valve), and the static pressure at both stations 5 and 8 (fig. 3) in both the left and right engines. The telemeter recorded data throughout the flight to a time of about 170 seconds.

Continuous-wave Doppler radar near the launching site was used to measure velocity of the test vehicle for the first 40 seconds of the flight. The flight path of the vehicle was obtained by NACA modified SCR 584 tracking radar.

A balloon carrying a radiosonde was released immediately after take-off to obtain atmospheric conditions.

TESTS AND METHODS

Preflight Tests

The tests were made in the preflight jet of the Langley Pilotless Aircraft Research Station at Wallops Island, Va. Nozzles which were 12 by 12 inches square were used for free-jet Mach numbers of 2.00 and 2.25. Round nozzles of 8-inch diameter were used for jet Mach numbers of 1.84, 2.06, and 2.21. The ram-jet inlet cowl was located within the Mach diamond or wedge of the nozzle. The model throughout all tests was at 0° angle of attack and 0° angle of yaw. The variation of static temperature and Reynolds number based upon the cowl entrance diameter of 4.42 inches is presented in table II. Approximate sea-level static pressure was maintained during the tests.

The average total-pressure recovery at stations 4 and 5 was determined in the cold-flow variable-exit tests by integration of the measured profiles as follows:

$$\frac{H}{H_0} = \frac{\int_0^1 H_l d\left(\frac{y}{r}\right)^2}{H_0}$$

The mass-flow ratio m/m_0 was obtained by use of the expression

$$\frac{m}{m_0} = \frac{\rho_5 A_5 V_5}{\rho_0 A_{cowl} V_0} = \frac{A_5 P_5 \int_0^1 M_l \sqrt{1 + \frac{\gamma - 1}{2} M_l^2}\, d\left(\frac{y}{r}\right)^2}{P_0 M_0 \sqrt{1 + \frac{\gamma - 1}{2} M_0^2} A_{cowl}}$$

The above expression was then used to determine average values of M_4 and M_5 by using faired values of m/m_0 and the measured values of the static pressure at stations 4 and 5.

In the tare-drag tests choking plugs were used which allowed determination of the choking area at the exit of the model. By substituting the pressure ratio and Mach number for $M = 1$ at station 10 and the pressure ratio for each free-jet Mach number in the mass-flow ratio equation, it becomes

$$\frac{m}{m_0} = K \frac{H_{10}}{H_0} \frac{A_{10}}{A_{cowl}}$$

where

$$K = \frac{1}{M_0} \left(\frac{1 + \frac{\gamma - 1}{2} M_0^2}{\frac{\gamma + 1}{2}} \right)^{\frac{\gamma+1}{2(\gamma-1)}}$$

The average total-pressure recovery H_7/H_0 was determined at station 7, and negligible losses were assumed between stations 7 and 10.

Again, from the faired values of m/m_0 with the measured values of static pressure, the Mach number was determined at stations 4 and 5.

In the reduction of the data it was found that the total-pressure measurement of the manifolded rake at station 4 in the combustion model yielded an error in total-pressure ratio H_4/H_0 of as much as 8 percent as compared to the measured total-pressure ratio H_7/H_0. The value of the total pressure at station 4 (and station 5 during combustion tests) was determined, therefore, from the previously discussed calculated Mach number and the measured static pressures.

Because stations 4 and 5 are not at exactly the same area in the combustion and cold-flow models, one-dimensional-area relations are used to correct the Mach numbers calculated at stations 4 and 5 in the combustion performance tests to the areas of stations 4 and 5 of the cold-flow model.

The combustion tests were made by using technical grade ethylene (C_2H_4) as a fuel. A thrust-drag balance was used to determine the thrust of the engine. Since the engine was large relative to the size of the nozzle, the external drag would be different from that which would be obtained in flight. This external drag – henceforth called tare drag – could be determined on the thrust-drag balance in cold-flow tests, as the engine air mass flow could be duplicated by the series of fixed-area plugs used. The thrust of the ram-jet engine is given, then, by (ref. 2)

$$F = X + D_t = G_{10} - P_0\left(\gamma_0 M_0^2 A_0 + A_{10}\right)$$

where the exit-jet propulsive force is

$$G_{10} = S_{a_9}\phi(M)W_a$$

where

$$W_a = mg$$

The ideal exit-jet propulsive force is

$$G_{10}' = S_{a_9}'\phi(M)W_a$$

and, therefore, air impulse efficiency is

$$\eta_i = \frac{G_{10}}{G_{10}'}$$

As shown in the appendix, the combustion efficiency is

$$\eta_c = \frac{\Delta h}{\frac{f}{a} h_c}$$

Ram-jet starting and fuel-regulation techniques employed for the combustion-performance tests were the same as outlined in reference 2. In addition, fuel supplied to the engine was passed through a hot-water jacket to keep the ethylene fuel within the critical temperature range.

Fuel was programmed to the engine in 5 to 7 steps in fuel rate, each step increase in fuel rate being held constant for approximately 1 second to permit fuel flow to attain equilibrium. Fuel rate was thus increased from a starting rate $\left(\frac{f}{a} \approx 0.02\right)$ until buzz occurred and then was decreased in steps until lean burnout was accomplished.

Flight Test

The flight test of the ram-jet vehicle was also conducted at the Langley Pilotless Aircraft Research Station at Wallops Island, Va. The vehicle was launched at a 60° elevation angle and was accelerated to $M_0 = 1.76$ by the double-rocket booster. Ignition of the ram jets occurred at $M_0 \approx 1.58$ approximately 2.5 seconds after take-off. Booster separation occurred at 3 seconds, and the test vehicle then accelerated to a velocity of 2,548 feet per second, corresponding to a peak Mach number of 2.61, at a time of 23.5 seconds. Combustion was sustained to an altitude of 63,600 feet. Burnout occurred at 36.11 and 36.38 seconds for the right and left engines, respectively, at a Mach number of $M_0 \approx 2.48$. The vehicle coasted to a peak altitude of approximately 105,000 feet. A trajectory of the flight is presented in figure 4 up to a time of 120 seconds. Mach number and time are indicated along the flight path.

The model throughout the flight flew along a zero-lift trajectory. The variation of the static-pressure ratio, static-temperature ratio (relative to standard sea-level conditions), and Reynolds number per foot as a function of the flight Mach number is presented in figure 5.

The Mach number of the model was determined by velocity measurement by continuous-wave Doppler radar. The flight path of the model was determined by NACA modified SCR 584 radar. The speed of sound was calculated from information obtained from a radiosonde balloon. Atmospheric pressure was checked by a static orifice on the missile body 12 diameters downstream from the base of the nose cone. The Mach number was further verified by a free-stream pitot stagnation probe.

Static pressure was measured at station 5 in both ram-jet engines. The mass flow into the engine was determined by $m = \rho_0 A_0 V_0$ where A_0 was obtained from the ground-test results by assuming no throttling. From the mass flow and the measured static pressure at station 5, the Mach number at station 5 was determined. From the pressure ratio corresponding to the Mach number, the total pressure was determined.

As the fuel control failed to operate as designed, but instead opened to the full-open position, ground tests were made on a similar fuel tank in which the control was operated as a quick-opening valve and a simulated fuel rate was determined. This simulated fuel rate was then used to determine the model weight change due to fuel consumption.

The net thrust, defined as the actual net propulsive force, was then determined from the longitudinal acceleration and the vehicle mass corrected for fuel consumption. Net thrust coefficients were then determined by using atmospheric conditions presented in figure 5. For performance evaluation, the external drag of the vehicle was assumed to be the same as the external drag of the test vehicle reported in reference 1. This assumption was made because the drag coefficients derived from the flight test of this report were not of sufficient accuracy. Since drag data could be obtained only after burnout, the drag forces were small because of the low dynamic pressures encountered at the high altitudes, and hence would have involved the use of accelerometer readings less than 1 percent of full-scale deflection. The flight test vehicle of this report is the same as the vehicle of reference 1 except that the cowl lip area of the engines is 25 percent greater. However, external cowl slopes were the same in the engines of both flight vehicles. The engines of this report, therefore, should have had less pressure drag. Estimates of this difference in pressure drag show a maximum possible error in $C_{D_{external}}$ of approximately 2 percent which results in a possible error in $C_{T_{gross}}$ of approximately 1 percent.

The difference in external-drag coefficient of the two flight vehicles is, therefore, not considered significant and the external-drag coefficient of the vehicle of reference 1 was then added to the net thrust coefficient to obtain gross thrust coefficient.

The computed fuel-air ratio of the flight was determined by

$$f/a = \frac{\sqrt{\frac{R_9 T_9}{\gamma_9 g}\left(\gamma_9 + 1\right)^2}}{S_{a_9}} - 1$$

where

$$S_{a_9} = S_{a_9}'\eta_i = \frac{F + P_0\left(\gamma_0 M_0^2 A_0 + A_{10}\right)}{\phi MW_a}$$

All quantities in the above equation could be obtained from the flight data or theoretically evaluated except η_i and A_0 for which ground-test values were used. For A_0, unthrottled ground-test values were used because air mass-flow spillage could not be measured in flight.

ACCURACY

Preflight Tests

Instruments used in these tests were accurate to ±1 percent of their full-scale range. By accounting for this error and also by observing the scatter of points in repeated tests, the magnitude of the possible error is believed to be within the following limits:

M_0	±0.01
H_4/H_0 and H_5/H_0	±0.02
m/m_0	±0.02
M_4 and M_5	±0.02
C_T	±0.02
f/a	±0.002
η_i	±0.025
η_c	±0.025

Flight Test

Telemetered data are accurate to ±2 percent of full-scale range. CW Doppler radar determined velocity, checked by a free-stream pitot stagnation probe, is accurate to ±1 percent at the maximum Mach number value of 2.61. Since air mass-flow spillage could not be measured in flight, an indeterminate error may exist in the fuel-air ratio at Mach

numbers below the design. The magnitude of the possible error is believed to be within the following limits:

M_0	± 0.02
H_5/H_0	± 0.04
C_T	± 0.04
f/a	± 0.004, M_0 = 2.13 to 2.61
	indeterminate, M_0 = 1.9 to 2.13

RESULTS AND DISCUSSION

Preflight Tests

The variation of total-pressure recovery with internal-flow Mach number at stations 4 and 5 and the total-pressure recovery between stations 4 and 5 is presented in figure 6 for the cold-flow variable-exit area tests at $M_0 = 2.00$ and 2.25 and at combustion performance Mach numbers of 1.84, 2.06, and 2.21. Good agreement is noted between the measured total-pressure recoveries of the cold-flow tests and the calculated total-pressure recoveries of the combustion performance tests. Generally, the total-pressure recovery increases in value as the internal Mach number is decreased. At free-jet Mach numbers of 1.84, 2.00, and 2.06, the internal Mach number can be reduced to a value where the total-pressure recovery no longer increases but levels off to a nearly constant value. (The total-pressure recovery decreases slightly with decreasing values of M_4 or M_5 for $M_0 = 2.06$.) This portion of the internal Mach number range corresponds to mass-flow spillage after the internal back pressure has forced the normal shock outside the inlet lip. The lowest value of internal Mach number is reached when buzz occurs. The total-pressure recovery between stations 4 and 5 is unity at the lower values of M_5 and decreases to a value of approximately 0.98 at a value of $M_5 = 0.287$.

The variation of mass-flow ratio with station Mach number M_4 is shown in figure 7. This figure shows that no reduction in mass-flow ratio was possible with this ram-jet engine without buzz occurring at free-jet Mach numbers of 2.21 and 2.25. M_4 could be reduced to a value of 0.27 at a free-jet Mach number of 2.21 in combustion tests and to a value of 0.26 at $M_0 = 2.25$ in cold-flow tests, at which points buzz occurred. Some reduction in mass flow was possible at $M_0 = 2.06$, 2.00, and 1.84, starting at a value of $M_4 \approx 0.29$. The greatest amount of mass-flow spillage occurred at $M_0 = 1.84$. The spillage region was found to be very transitory with slight changes in back pressure causing appreciable reduction

in M_4; therefore, the values of M_4 at which buzz begins are only approximate. In the combustion tests, rough burning occurred just before buzz, causing pulsations in both thrust and pressure readings. Hence, errors as great as those stated in the section entitled "Accuracy" in both m/m_0 and M_4 are possible and likely in the mass-flow-spillage region of these data.

In the portion of figure 7 where m/m_0 is constant for the various free-jet Mach numbers, good agreement is noted with the theoretical values of A_0/A_{cowl} obtained by the method of reference 2.

The radial distribution of Mach number at stations 4 and 5 at free-jet Mach numbers of 2.00 and 2.25 in cold-flow tests and at station 4 at $M_0 = 2.21$ in combustion performance tests are shown in figure 8. The distribution profiles show a low Mach number region or wake at both the outer walls and at the innerbody for most of the tests. At $M_0 = 2.25$ and $\frac{H_4}{H_0} = 0.66$ in cold tests and at $M_0 = 2.21$ and $\frac{H_4}{H_0} = 0.63$ in combustion tests, the profile has changed shape abruptly to a separated flow region off the central body. Comparisons of these and the other profiles of the cold tests and combustion tests show that the profiles are quite similar and apparently not affected by combustion.

Static-pressure variation within the inlet at free-jet Mach numbers of 2.00 and 2.25 is shown in figure 9 by the variation in static-pressure ratio for a range of static-pressure orifice locations on the inlet central body for various total-pressure recoveries.

At $M_0 = 2.00$ and $\frac{H_5}{H_0} = 0.81$, the static-pressure profile increases to a peak value near the inlet minimum area and decreases in value further downstream. Since the inlet had a contraction ratio of $\frac{A_e}{A_3} = 1.16$, the inlet could not "start" at this Mach number and a shock is located just inside the inlet lip, indicated by the pressure of the first few orifices, all being above the theoretical cone surface pressure ratio. Behind this shock, the throat contraction again causes the internal flow to become sonic, and past the inlet minimum area the flow becomes supersonic, as indicated by the decrease in value of P_l/P_0. As the back pressure is increased, a normal shock, which was previously located at some station past the last pressure orifice, is now evident at $\frac{H_5}{H_0} = 0.82$ by the abrupt rise in P_l/P_0. As the back pressure is further increased, the shock is moved further toward the minimum area and finally outside the inlet at $\frac{H_5}{H_0} = 0.85$.

At $M_0 = 2.25$ the inlet contraction ratio no longer prevents "starting" and the first two orifice pressure ratios closely check theoretical cone-surface pressure ratio at all test conditions. The flow inside the inlet is supersonic with expansion waves and reflected oblique shock waves causing the sharp breaks and changes in the slope of the static-pressure profile. Again as the back pressure is increased, the normal shock is forced upstream toward the minimum area, and then past the throat to outside the inlet and buzz begins.

Maximum total-pressure recovery for the various test free-jet Mach numbers is presented in figure 10. A value of $\frac{H_4}{H_0} = 0.87$ was attained at the minimum free-jet Mach number of 1.84 in combustion performance tests, whereas a value of $\frac{H_4}{H_0} = 0.78$ was attained in cold-flow tests at the maximum free-jet Mach number of 2.25. The differences shown between cold-flow and combustion performance tests are believed to be due to experimental methods and reduction of the data and are within the experimental accuracy. A test point at $M_0 = 2.00$ from reference 2 of an inlet with 20° semiangle cone but with an entrance area 25 percent smaller indicates excellent agreement with the value of total-pressure recovery of the combustion performance tests.

Thrust coefficient C_T as a function of fuel-air ratio f/a is presented in figure 11 for free-jet Mach numbers 1.84, 2.06, and 2.21. Rich burnout was not obtained in any of the tests because fuel rate was decreased to prevent damage to the engine and thrust stand whenever violent buzz conditions were reached. Maximum thrust coefficients and corresponding fuel-air ratios for the various test Mach numbers are presented in the following table:

M	f/a	C_T
1.84	0.083	0.77
2.06	.087	.87
2.21	.087	.91

Maximum thrust coefficients were reached at the beginning of buzz. Lean burnout was accomplished, but the fuel-air ratios at which it occurred could not be accurately evaluated because of the reduced accuracy of the fuel-measuring instruments at low fuel rates.

Air spillage is evident at Mach numbers 1.84 and 2.06 by the change in the slope of the curve beginning at $\frac{f}{a} \approx 0.05$ and $\frac{f}{a} \approx 0.06$, respectively. This slope change is more noticeable at Mach number 2.06 than it is at Mach number 1.84. At Mach number 2.06 the normal shock is just inside the entrance of the supersonic diffuser prior to spillage. After spillage begins, the normal shock moves ahead of the entrance with a resulting abrupt increase in tare drag of approximately 3.5 percent. At $M = 1.84$ the contraction ratio is such that the normal shock is always ahead of the diffuser entrance, and, therefore, spillage tends only to move the normal shock forward with a more gradual increase in tare drag.

Since the tests at Mach number 2.06 were near the design Mach number of the inlet, the higher values of thrust coefficient for the same f/a below $\frac{f}{a} = 0.07$ would be expected because of increased engine cycle efficiency.

Air impulse efficiency η_i and combustion efficiency η_c as a function of the fuel-air ratio are presented in figure 12 for free-jet Mach numbers of 1.84, 2.06, and 2.21. Small differences in both η_i and η_c were found for the three test Mach numbers. Maximum values of air impulse efficiency of 96 percent and combustion efficiency of 84 percent, were attained at $\frac{f}{a} \approx 0.025$. Both η_i and η_c decrease in value from these maximum values with increasing f/a.

The economy of the engine, the specific fuel consumption, as a function of the fuel-air ratio is also presented in figure 12. The most economical operating point occurs near $\frac{f}{a} \approx 0.035$ at a value of specific fuel consumption of 2.4 with increasing values of specific fuel consumption at values of f/a below and above this operating point. The specific fuel consumption increases in value more gradually at $M_0 = 2.21$ with increasing values of f/a and is, therefore, a more economical cruise Mach number than 1.84 or 2.06.

Total pressure recovery H_4/H_0 as a function of thrust coefficient C_T is presented in figure 13. The data show an approximately linear variation of H_4/H_0 with C_T for all three test Mach numbers.

Static pressure ratios P_5/H_0 at the diffuser exit station, and P_8/H_0 at a combustion-chamber station as a function of thrust coefficient C_T are presented in figure 14. The data show an approximately linear variation of both static pressure ratios with C_T similar to the previously noted total-pressure-recovery variation with C_T. Solid points of reference 3, the flight-test performance of this engine, show good agreement.

Thrust coefficient as a function of free-jet Mach number for a range of f/a from 0.02 to 0.08 is presented in figure 15. The thrust coefficient C_T reaches a maximum value for nearly all fuel-air ratios at $M_0 = 2.13$, the design Mach number of the inlet.

The engine of these tests was a modification of the engine of reference 2, consisting of a 25-percent increase in entrance area to improve the thrust performance. Data test points from reference 2 at $\frac{f}{a} = 0.06$ and 0.08 at free-jet Mach numbers of 1.8 and 2.0 indicate thrust performance was increased. The engine of reference 2 reached a value of $C_T = 0.69$ at $\frac{f}{a} = 0.06$ and $C_T = 0.80$ at $\frac{f}{a} = 0.08$ at a free-jet Mach number of 2.00. The modified engine reaches values of $C_T = 0.83$ at $\frac{f}{a} = 0.06$ and $C_T = 0.85$ at $\frac{f}{a} = 0.08$, representing increases in C_T at $M_0 = 2.00$ of 20.3 and 6.2 percent, respectively.

In figure 16, the combustor force coefficient, C_c is presented as a function of the diffuser exit Mach number M_5. This dimensionless coefficient, which expresses the ratio of the force at the exit of the combustion chamber to the force just before combustion is independent of free-stream Mach number and total temperature and has a linear variation with diffuser exit Mach number. It, therefore, appears as a parameter which can be used to predict the thrust performance of other ram-jet engines by making cold-flow inlet tests, as

$$F = G_{10} - P_0\left(\gamma_0 M_0^2 A_0 + A_{10}\right)$$

By determining the total-pressure recovery, the diffuser exit Mach number, and the entrance conditions expressed in the above equation of any similar type of ram-jet inlet in cold-flow tests, the combustor force coefficient can be used to predict the performance of other ram-jet engines, assuming the engine to use a "donut" burner and ethylene fuel.

It is beyond the scope of this paper to show the analysis of this parameter. For additional data and analysis see reference 4.

Typical shadowgraph flow patterns of the ram-jet inlet for the range of free-jet Mach numbers investigated are presented in figure 17. Forward movement of the normal shock is evident prior to the beginning of buzz at free-jet Mach numbers of 1.84 and 2.06 in combustion performance tests and at a Mach number of 2.00 in cold-flow tests. Mass-flow reduction is not possible at free-jet Mach numbers of 2.21 and 2.25. In these cases buzz occurs when the normal shock is first forced from the inlet minimum area to a position at the entrance to the inlet. A number of random exposures during the buzz cycle are presented for each free-jet Mach number.

Flight Test

Static-pressure ratios P_5/H_0 and P_8/H_0 and total-pressure recovery H_5/H_0 are presented as a function of free-stream Mach number in figure 18 for the flight-test model. At a Mach number of 1.92 to a Mach number of 2.28, the attitude of the model was such that it "blanketed" the antenna signal with respect to the ground-receiving station, and the telemeter signal as a result was lost during this range of Mach numbers. Above $M_0 = 2.28$ and for the rest of the flight, the telemeter signal was uninterrupted. The data presented in this figure and all figures requiring calculations from telemeter data are faired through this Mach number range.

Ground-test maximum values of H_5/H_0 are shown in the total-pressure-recovery plot of figure 18, indicating that the engines were at buzz conditions for $M_0 \approx 1.76$ to $M_0 \approx 1.85$. This is confirmed by the telemeter record, which showed the characteristic cyclic pressure variation at buzz which was found in the ground test of this engine. In spite of the increased drag that results from buzz condition of the engines at these Mach numbers, the engines accelerated the vehicle to higher Mach numbers, and buzz ceased. Nearly maximum total-pressure recovery was measured from $M_0 = 1.76$ to $M_0 = 2.21$. After $M_0 = 2.21$, the fuel rate decreased to a value such that the back pressure began to decrease and the total-pressure-recovery values decreased at a faster rate for the rest of the flight. A pressure-recovery value of 0.43 was calculated for the M_{max} value of 2.61. Burnout of the ram-jet engines is indicated by the sharp break in both static-pressure ratio and total-pressure recovery at $M_0 = 2.48$.

The calculated Mach number at station 5 is presented as a function of the free-stream Mach number in figure 19. The diffuser exit Mach number varied from a minimum value of 0.215 to a maximum of 0.392. Recorded pressure traces indicate smooth and stable operation over this wide range of combustion-chamber entrance Mach numbers.

Thrust coefficient $C_{T_{net}}$ and $C_{T_{gross}}$, drag coefficient (from ref. 1), and fuel-air ratio are presented as a function of the free-stream Mach number in figure 20. Gross thrust coefficient is presented based on both the body area and the area of two ram-jet engines. The calculated net thrust coefficient was added to the external drag coefficient to obtain the gross thrust coefficient.

A maximum gross thrust coefficient of 0.78, based upon the two engine areas was reached at $M_0 = 2.36$. The curves reverse after $M_{0_{max}} = 2.61$ because of the decrease in flight speed while the engines are operating at decreased thrust.

Calculated fuel-air ratio is also presented in figure 20 as a function of the free-stream Mach number. Because the engine was at buzz condition at the lower values of Mach numbers, f/a could not be calculated below $M_0 = 1.90$. A maximum value of fuel-air ratio was reached of 0.042 at $M_0 = 2.35$ and a minimum value of 0.022 was reached at burnout at $M_0 = 2.48$.

Integration of the ground-test fuel rate from ignition to burnout of the ram-jet engines yields a value of 18.65 pounds of fuel used. Integration of the calculated fuel rate, assuming complete heat release over the same period, yields a value of 13.65 pounds of fuel. The ratio of fuel consumption calculated for complete heat release to fuel consumed by the engines give an overall combustion efficiency, η_c, of 73 percent.

Integration of the gross thrust over the same time interval yields a value of total impulse of 23,214 pound-seconds. By dividing this total impulse by the 18.65 pounds of fuel (as determined by integration of the ground-test fuel rate) an overall specific impulse S_f of 1,246 seconds was obtained.

SUMMARY OF RESULTS

Preflight Tests

The following results were obtained in cold-flow and combustion performance tests of a 6.5-inch-diameter, 20° semiangle conical ram-jet engine for a range of free-jet Mach numbers from 1.84 to 2.25:

(1) Maximum total-pressure recoveries of 0.88, 0.80, and 0.77 were obtained at free-jet Mach numbers of 1.84, 2.06, and 2.21, respectively, in combustion performance tests. Maximum total-pressure recoveries of 0.85 and 0.78 were obtained at free-jet Mach numbers of 2.00 and 2.25, respectively, in cold-flow tests.

(2) Maximum thrust coefficients of 0.77 at a fuel-air ratio of f/a of 0.082, 0.87 at $\frac{f}{a} = 0.086$, and 0.91 at $\frac{f}{a} = 0.087$ at free-jet Mach numbers of 1.84, 2.06, and 2.21, respectively, were obtained. The thrust coefficient increased in value with increasing total-pressure recovery until the upper limit was reached at the beginning of buzz.

(3) Maximum values of air impulse efficiency and combustion efficiency were 96 and 84 percent, respectively, near a fuel-air ratio of 0.025 and were relatively independent of free-jet Mach number.

(4) The lowest value of specific fuel consumption was 2.4 at $\frac{f}{a} = 0.035$ at a free-jet Mach number of 2.06.

(5) Increases in thrust coefficient of 20.3 percent and 6.2 percent at fuel-air ratios of 0.06 and 0.08, respectively, were found at a Mach number of 2.00 over values of thrust coefficient attained with an engine of identical design except for a 25-percent-smaller capture area.

Flight Test

In this flight investigation of a ram-jet test vehicle, the following results were obtained:

(1) Both ram-jet engines operated satisfactorily at altitudes from 1,400 to 63,600 feet and over a Mach number range from 1.74 to 2.61.

(2) The ram-jet engines buzzed from a free-stream Mach number of approximately 1.76 to a free-stream Mach number of approximately 1.85; however, the engines were able to sustain combustion and accelerated the vehicle to higher Mach numbers where buzz ceased.

(3) A maximum gross thrust coefficient based on the two engine areas (0.462 square foot) of 0.78 was reached at a free-stream Mach number of 2.36.

(4) An overall combustion efficiency of 73 percent and an overall fuel specific impulse of 1,246 seconds were calculated for the flight.

Langley Aeronautical Laboratory,
National Advisory Committee for Aeronautics,
Langley Field, Va., August 24, 1953.

APPENDIX

DETERMINATION OF COMBUSTION EFFICIENCY

The combustion efficiency is defined as

$$\eta_c = \frac{\Delta h}{W_f h_c}$$

For constant pressure combustion the heat release as a function of the temperature rise is

$$\Delta h = \left(W_a + W_f\right)\left[\left(C_P\right)_c\left(T_s\right)_a\right] - W_a\left[\left(C_P\right)_m\left(T_s\right)_b\right]$$

Then,

$$\eta_c = \frac{\left(1 + \frac{f}{a}\right)\left(C_P\right)_c\left(T_s\right)_a - \left(C_P\right)_m\left(T_s\right)_b}{\frac{f}{a}h_c}$$

At throat station a, M = 1.00. Then,

$$T_s = T + T\left(\frac{\gamma - 1}{2}\right)$$

$$C_P = \frac{\gamma R}{\left(\gamma - 1\right)J}$$

Therefore,

$$\left(C_P\right)_c\left(T_s\right)_a = \left(C_P\right)_c T_a + \frac{\gamma_a R}{2J} T_a$$

Since from reference 5

$$\bar{C}_P = \frac{\int C_P \, dT}{(T_s)_a - (T_s)_b}$$

If the enthalpy of air is arbitrarily taken as zero at 540° R, the combustion efficiency becomes

$$\eta_c = \frac{\left(1 + \frac{f}{a}\right)(C_P)_c(T_a - 540) + \frac{\gamma_a R T_a}{2J} - (\bar{C}_P)_m\left[(T_s)_b - 540\right]}{\frac{f}{a}h_c}$$

In the calculation of combustion efficiency from the above equation, theoretical values were calculated for R and γ_a along with the assumption that injection fuel temperature was the same as the air inlet temperature with a datum of 540° R. Results compared favorably with η_c as obtained from charts of reference 6.

REFERENCES

1. Faget, Maxime A., and Dettwyler, H. Rudolph: Initial Flight Investigation of a Twin-Engine Supersonic Ram Jet. NACA RM L50H10, 1950.

2. Faget, Maxime A., Watson, Raymond S., and Bartlett, Walter A., Jr.: Free-Jet Tests of a 6.5-Inch-Diameter Ram-Jet Engine at Mach Numbers of 1.81 and 2.00. NACA RM L50L06, 1951.

3. Dettwyler, H. Rudolph, and Bond, Aleck C.: Flight Performance of a Twin-Engine Supersonic Ram Jet From 2,300 to 67,200 Feet Altitude. NACA RM L50L27, 1951.

4. Dettwyler, H. Rudolph, and Faget, Maxime A.: Engineering Method of Ram-Jet Thrust Determination Based on Experimentally Obtained Combustor Parameters. NACA RM L53E21, 1953.

5. Fricke, Edwin F.: Statistical Thermodynamics Applied to Chemical Kinetics of Combustion. Rep. No. EDR-22-407, Republic Aviation Corp., Oct. 1, 1947.

6. Turner, L. Richard, and Lord, Albert M.: Thermodynamic Charts for the Computation of Combustion and Mixture Temperatures at Constant Pressure. NACA TN 1086, 1946.

TABLE I

COORDINATES OF THE RAM-JET INLET COWL AND CENTRAL BODY

Inlet-cowl coordinates			Central-body coordinates	
Station, in. from cone tip	Radius, in.		Station, in. from cone tip	Radius, in.
	External	Internal		
3.020	2.215	2.210	0	0
3.170	2.270			|
	|			(a)
	|			|
	|		3.500	1.272
	|		3.600	1.316
	(a)		3.700	1.338
	|		3.800	1.356
	|		3.900	1.376
	|		4.000	1.390
	|	(a)	4.120	1.400
13.000	3.300	|	4.620	1.438
	|	|	5.120	1.468
	|	|	5.620	1.490
	|	|	6.120	1.504
	|	|	6.620	1.510
	(a)	|	7.000	1.510
	|	|	8.000	1.500
	|	|	9.000	1.480
	|	|	10.000	1.440
	|	|	11.000	1.380
23.563	3.300	2.970	12.000	1.310
		(a)	13.000	1.240
25.563		3.250	14.000	1.170

NACA

[a]Straight-line variation between stations.

TABLE II

GROUND TESTS:

STATIC TEMPERATURE AND REYNOLDS NUMBER RANGE

Free-jet Mach number	Static temperature range, ^{o}F	Reynolds number, based on inlet diameter
1.84	65 to 77	4.62 to 4.73 x 10^{6}
2.00	0 to 10	5.92 to 6.13
2.06	45 to 69	5.27 to 5.58
2.21	27 to 47	6.62 to 6.87
2.25	0 to 14	5.98 to 6.28

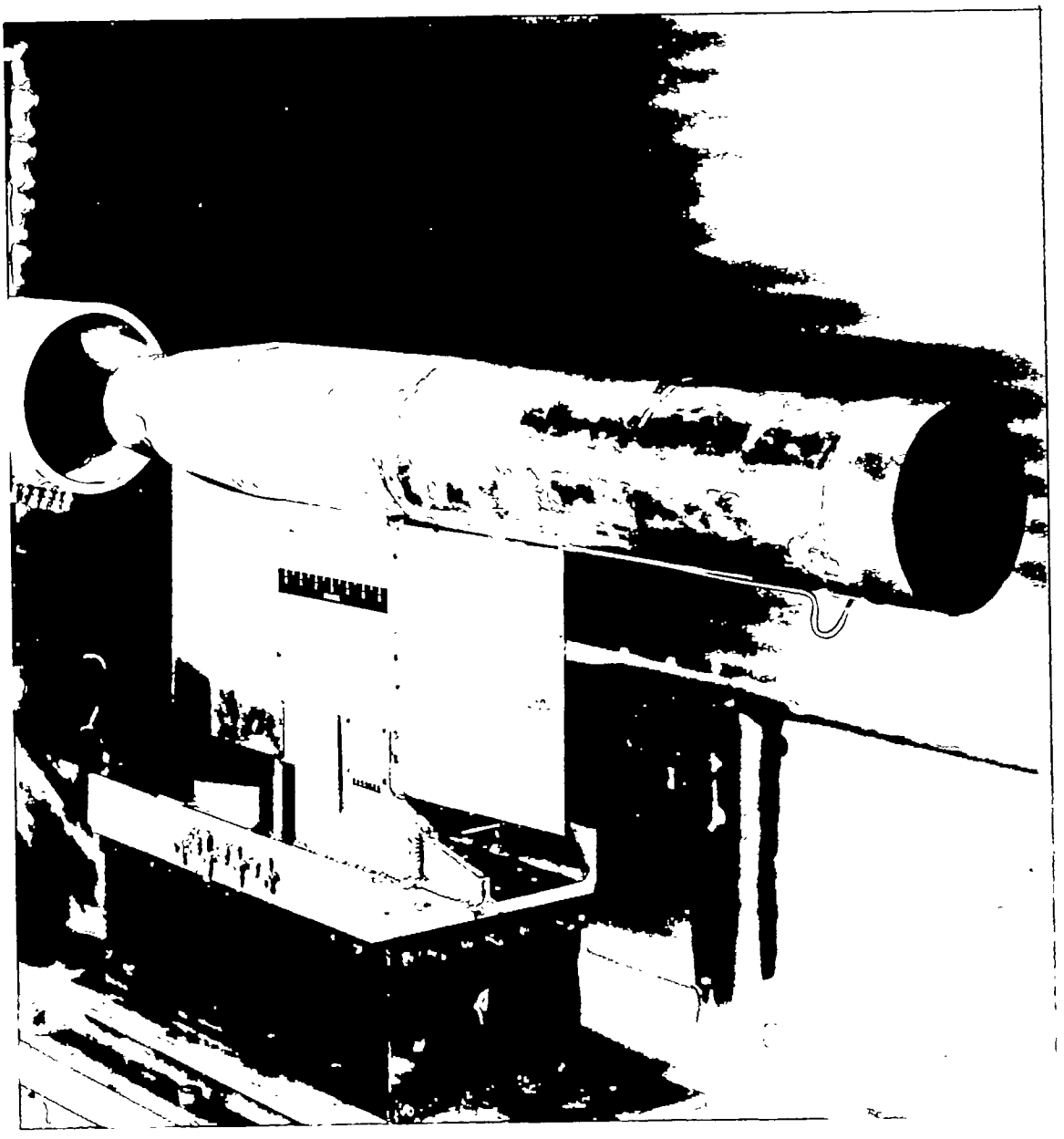

L-76704

(a) Ram-jet engine mounted on thrust-drag stand for combustion tests.

Figure 1.- The ram-jet test configurations.

L-76700

(b) Ram-jet engine fitted with fixed-exit-area tail plug for cold-flow tests.

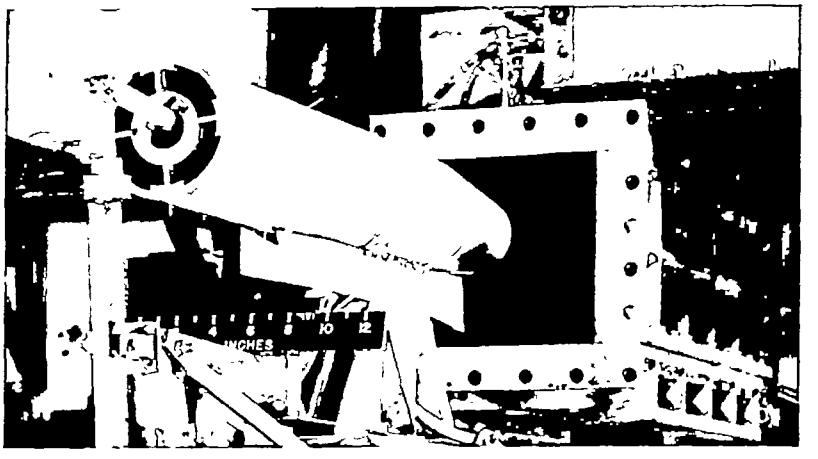

L-68520

(c) Variable-exit-area cold-test installation.

Figure 1.- Continued.

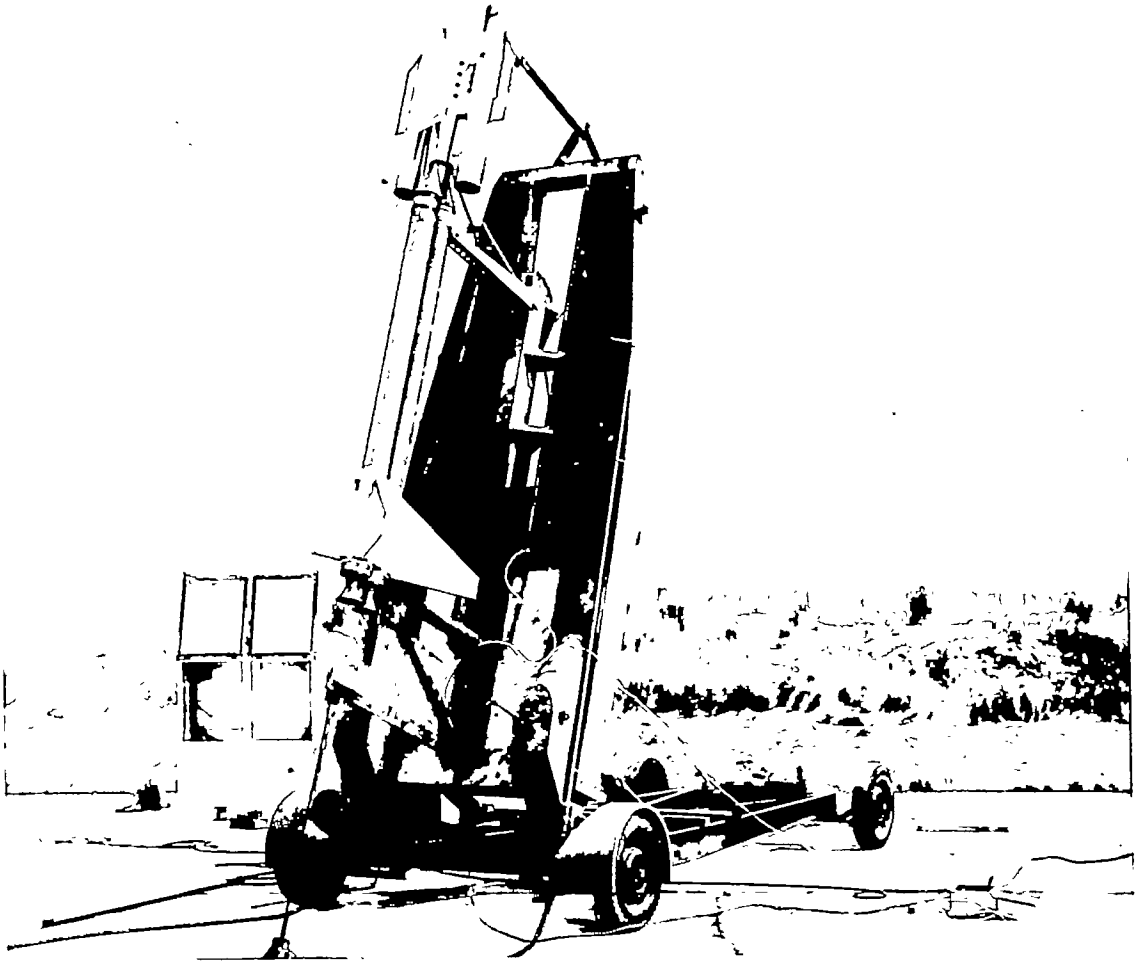

L-72448

(d) Ram-jet flight test model and double-rocket booster unit in launching attitude.

Figure 1.- Concluded.

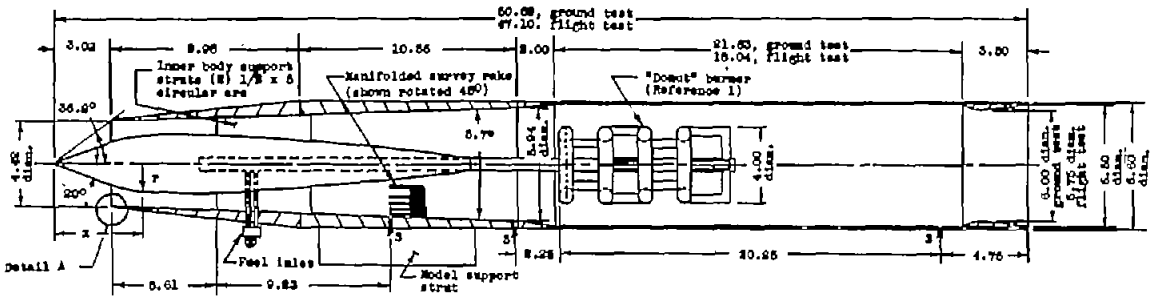

(a) Combustion performance test arrangement.

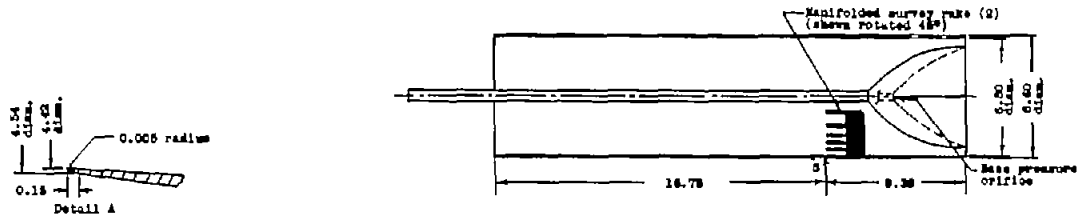

(b) Fixed-exit-area cold test arrangement.

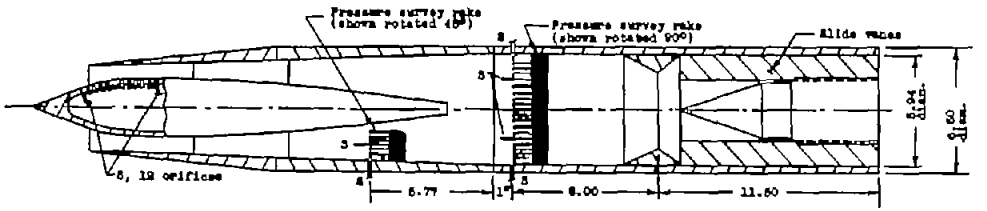

(c) Variable-exit-area cold test arrangement.

Figure 2.- Ram-jet model test configurations showing principal dimensions and pressure measuring stations. S denotes static orifice. All dimensions are in inches.

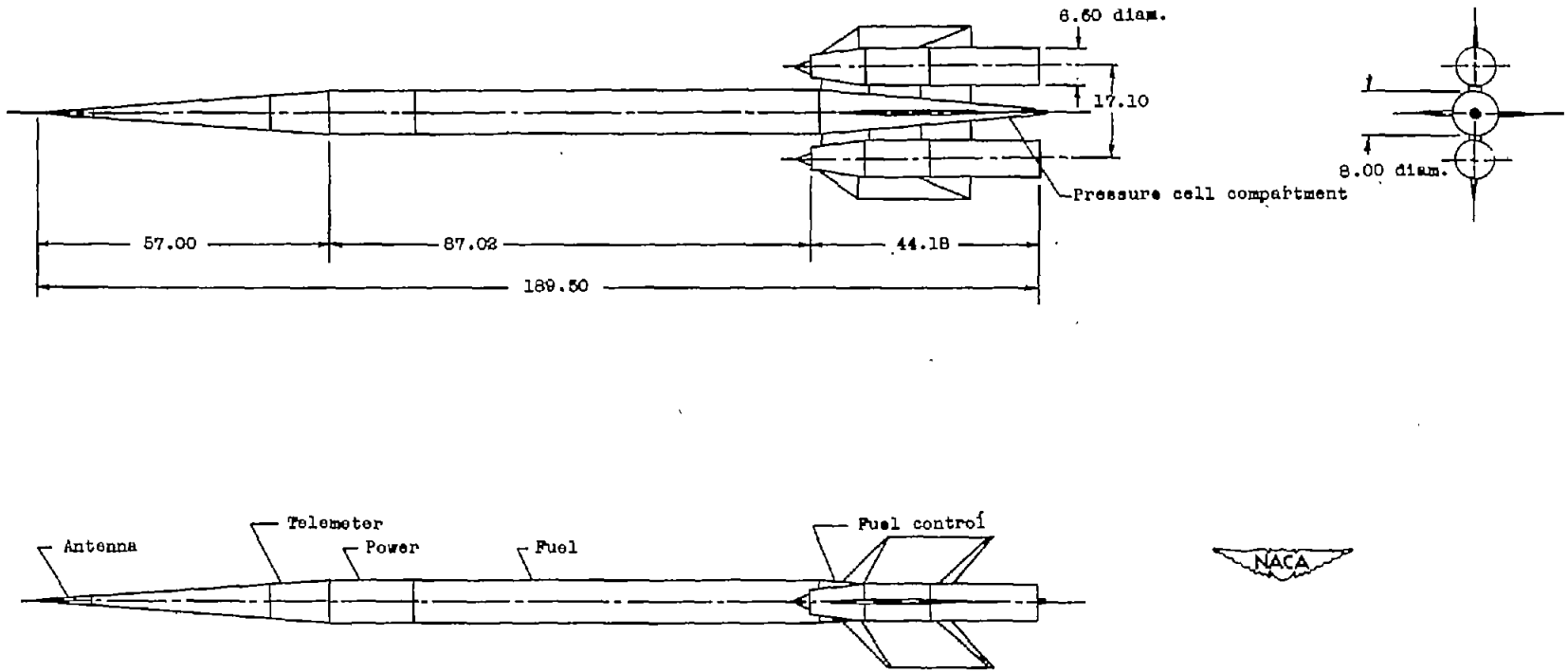

(d) General arrangement of flight test vehicle. All dimensions are in inches.

Figure 2.- Continued.

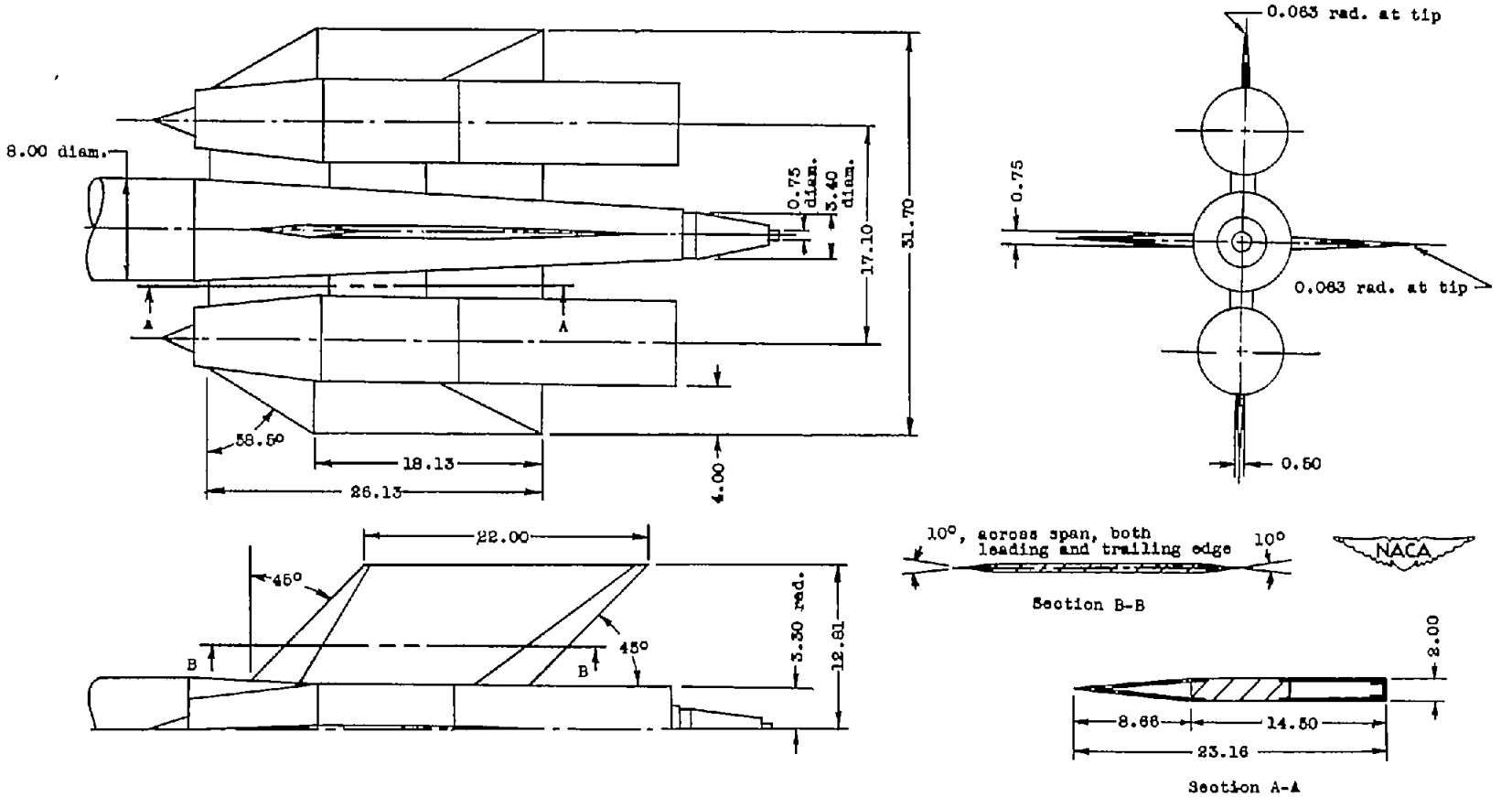

(e) Details of flight-vehicle fins and engines. All dimensions are in inches.

Figure 2.- Concluded.

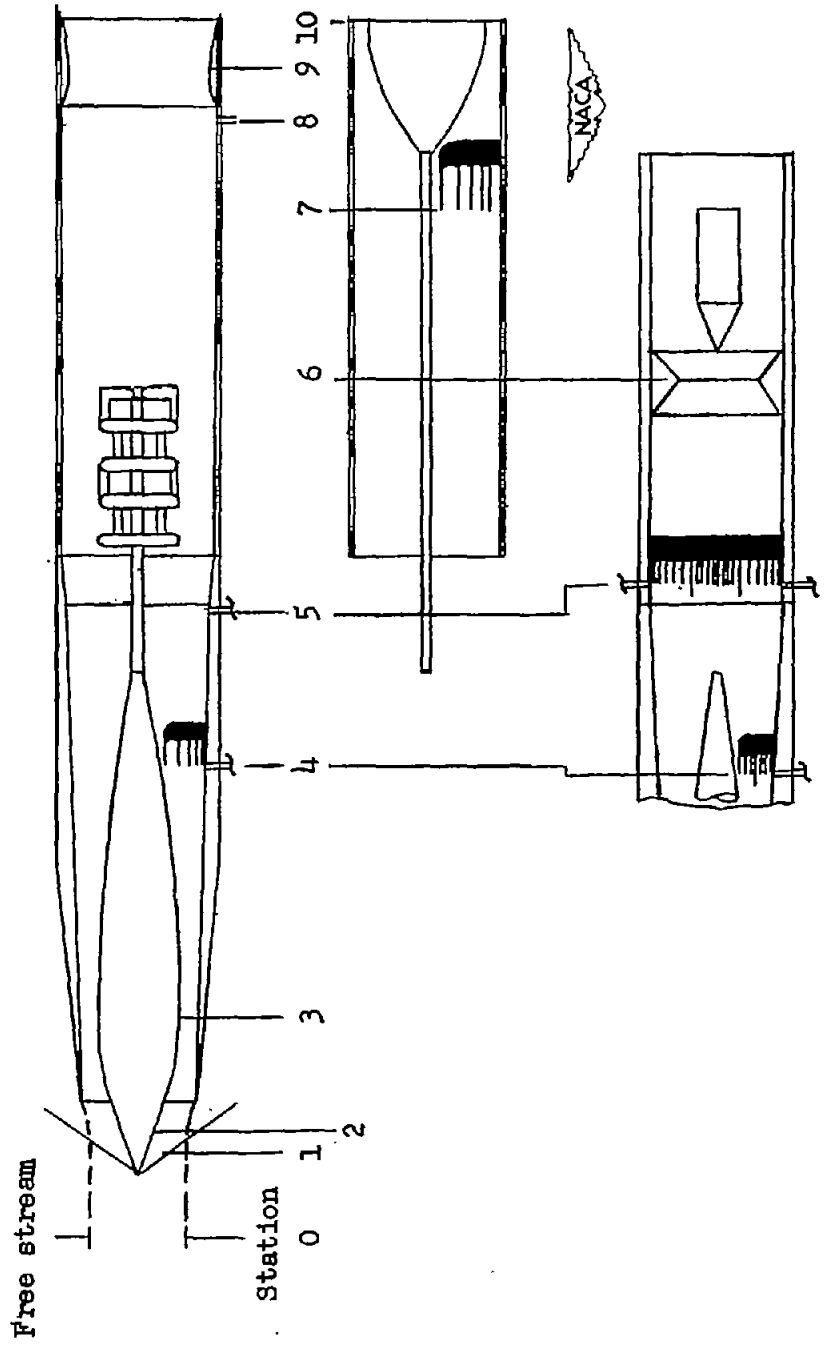

Figure 3.- Station notation for ram-jet combustion and cold-flow test arrangements.

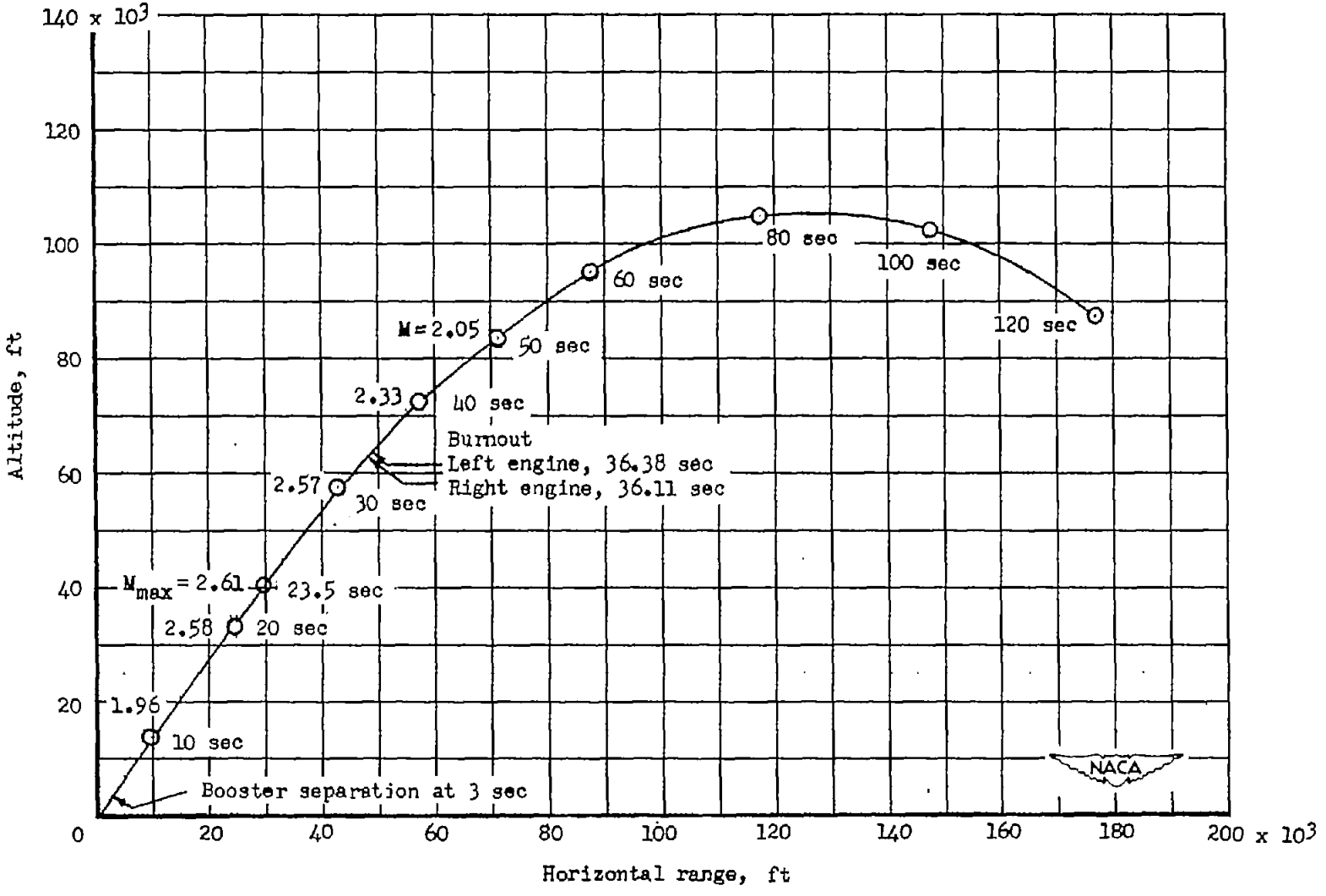

Figure 4.- Flight trajectory of ram-jet vehicle obtained by NACA modified SCR 584 radar.

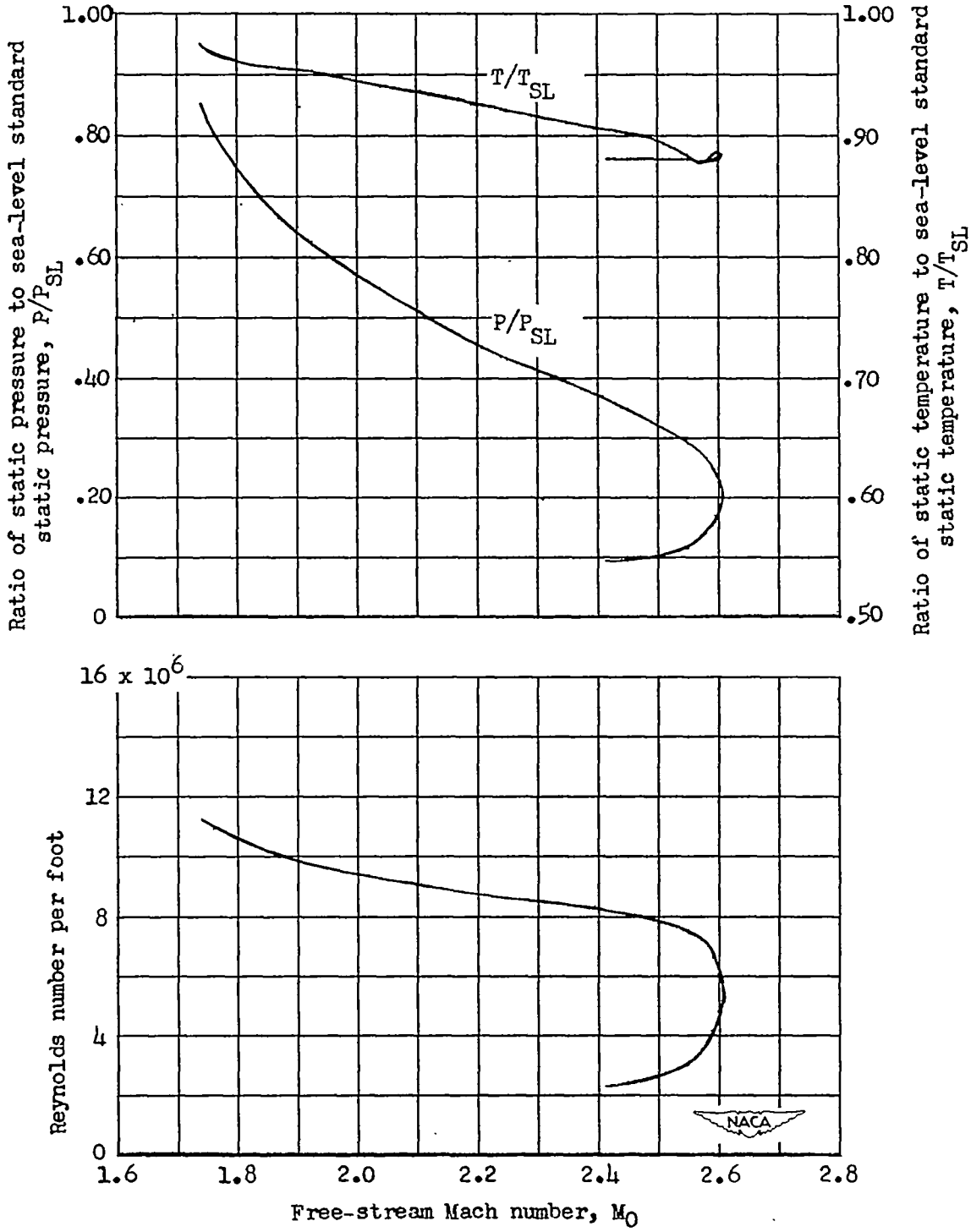

Figure 5.- Static-pressure ratio, static-temperature ratio, and Reynolds number per foot as a function of free-stream Mach number for the flight test model.

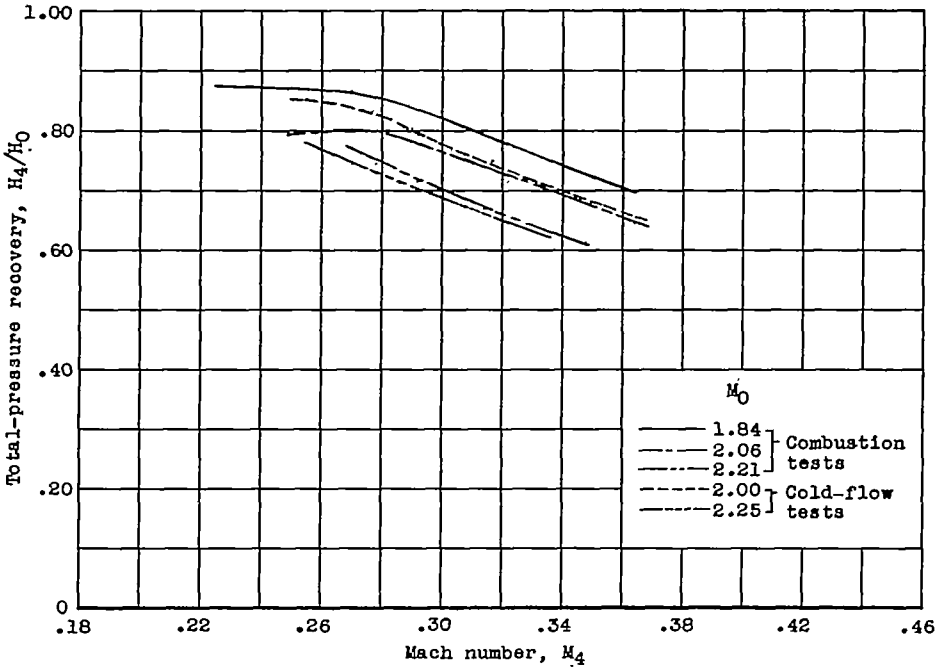

(a) Station 4.

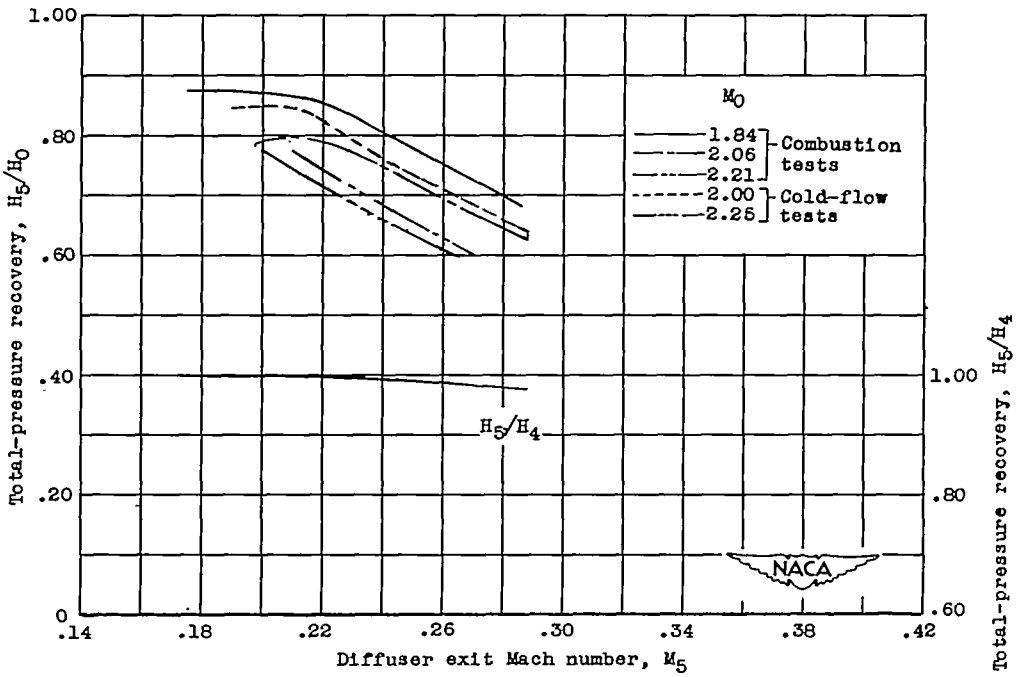

(b) Diffuser exit, station 5.

Figure 6.- Total-pressure recovery at and between stations 4 and 5 as a function of the station Mach numbers as obtained in preflight tests.

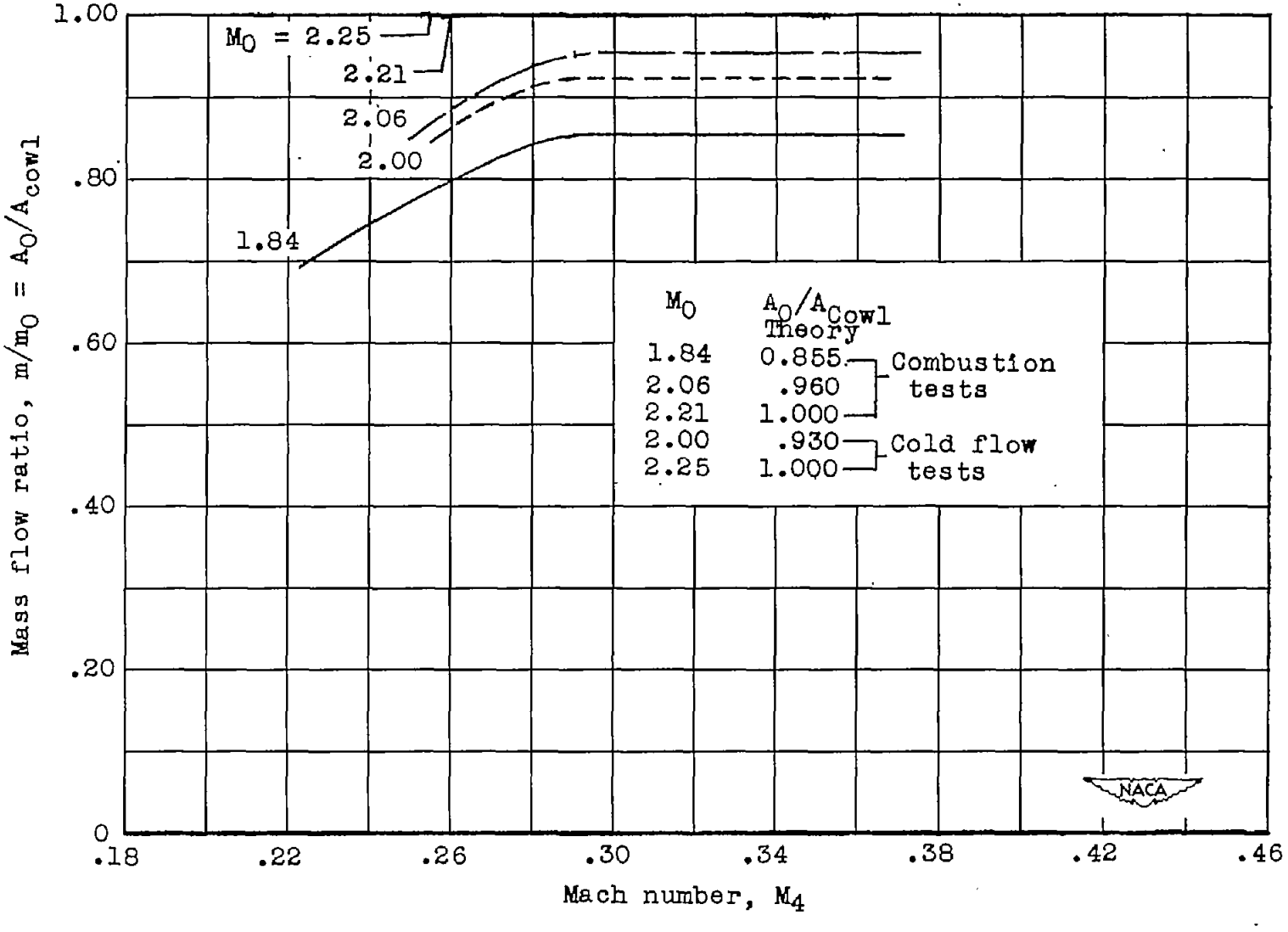

Figure 7.- Mass-flow ratio as a function of the Mach number at station 4.

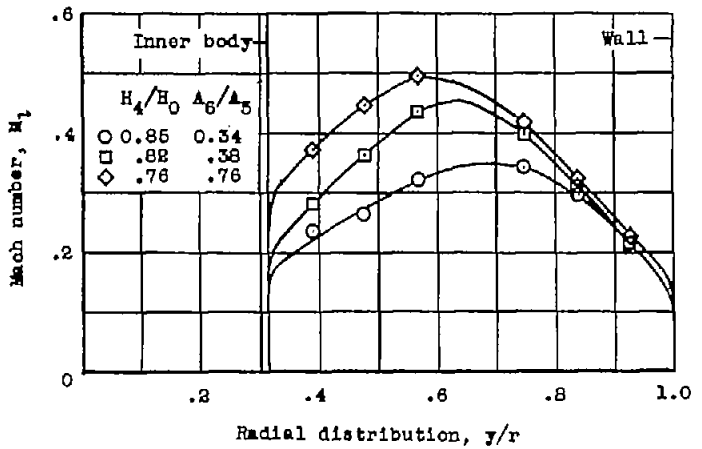

(a) M_0 = 2.00; rake station 4; cold flow.

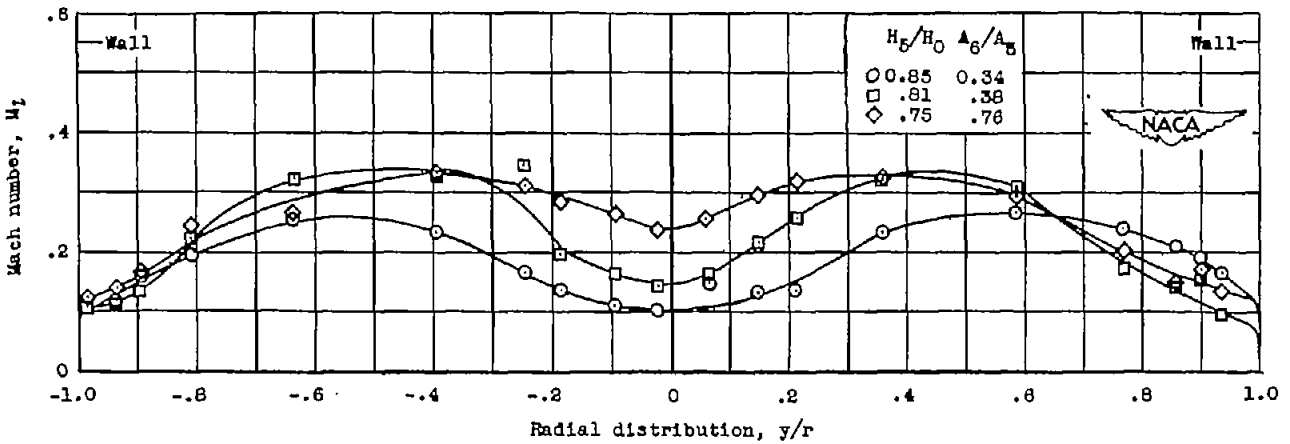

(b) M_0 = 2.00; rake station 5; cold flow.

Figure 8.- Mach number distribution at rake station.

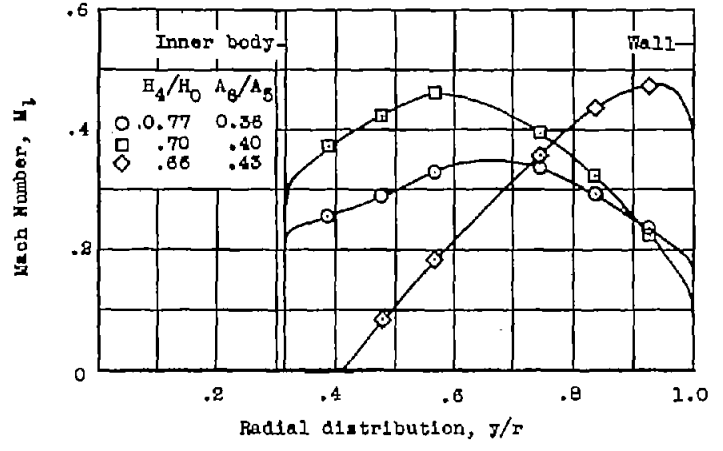

(c) M_0 = 2.25; rake station 4; cold flow.

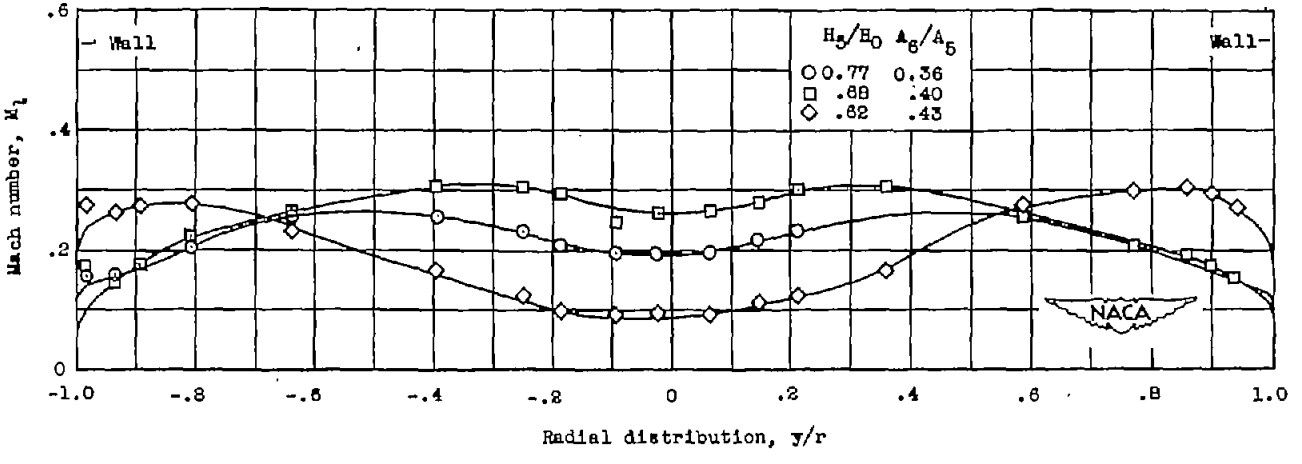

(d) M_0 = 2.25; rake station 5; cold flow.

Figure 8.- Continued.

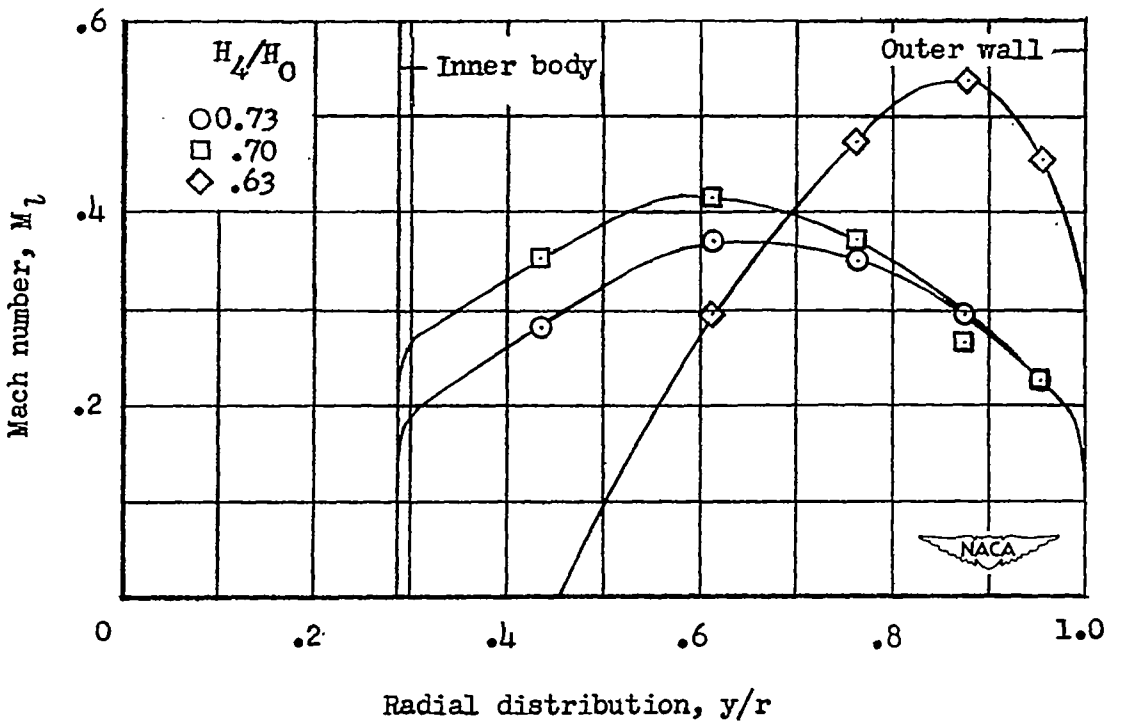

(e) M_0 = 2.21; rake station 4; combustion tests.

Figure 8.- Concluded.

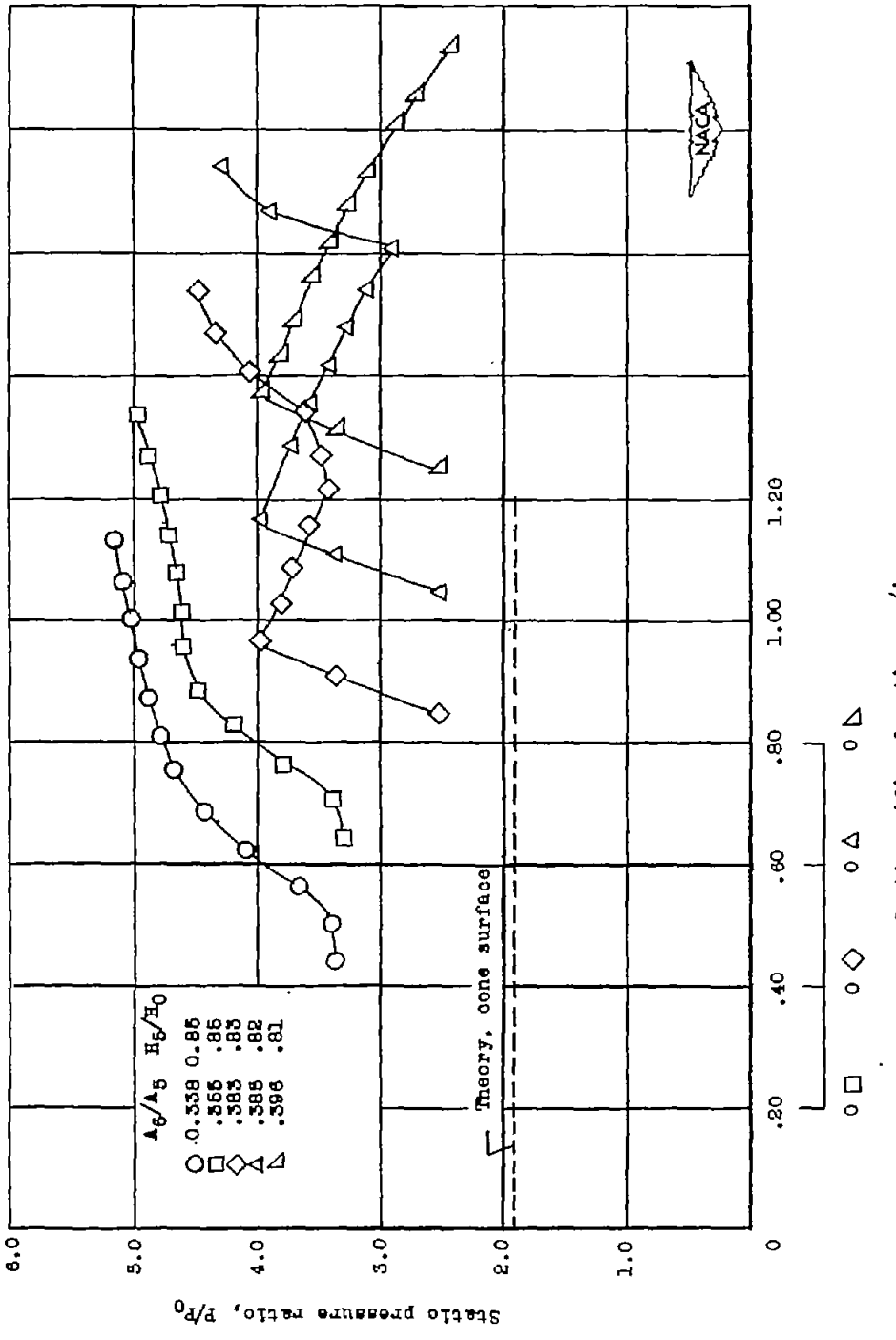

(a) $M_0 = 2.00$.

Figure 9.- Relation between the static-pressure ratio on the innerbody and the static-orifice location (measured from cone tip).

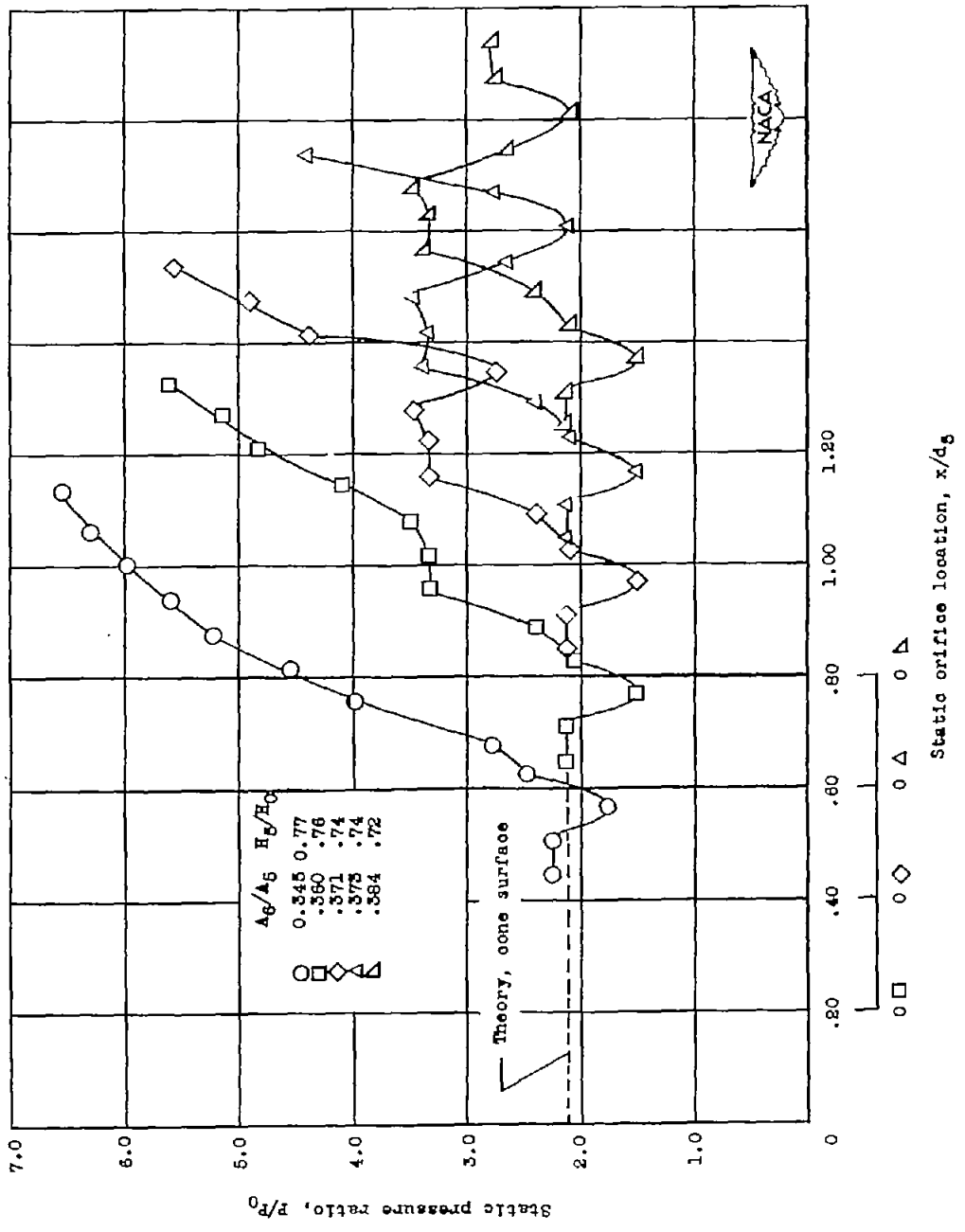

(b) $M_0 = 2.25$.

Figure 9.- Concluded.

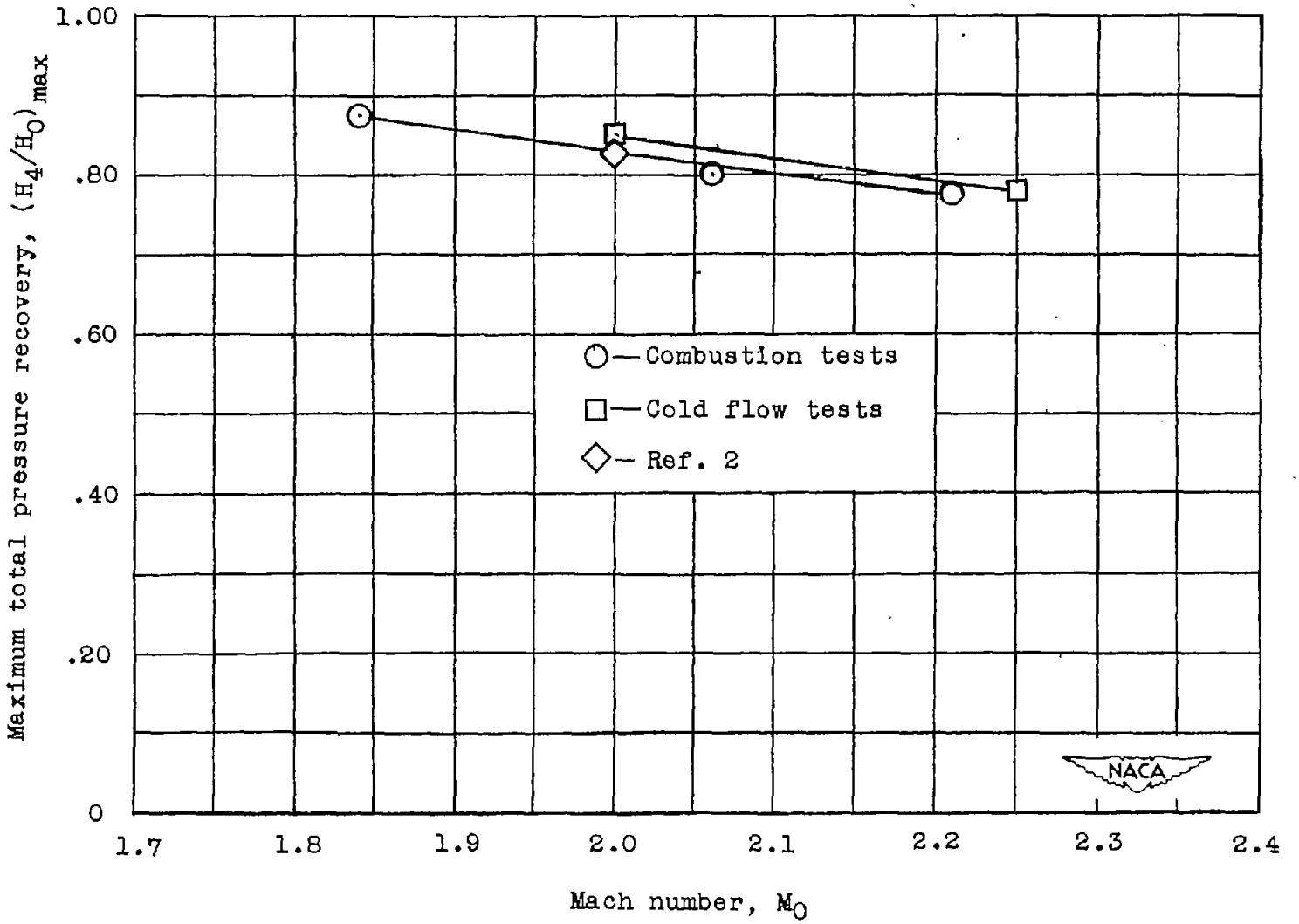

Figure 10.- The variation of maximum total-pressure recovery with free-jet Mach number in both cold and combustion tests.

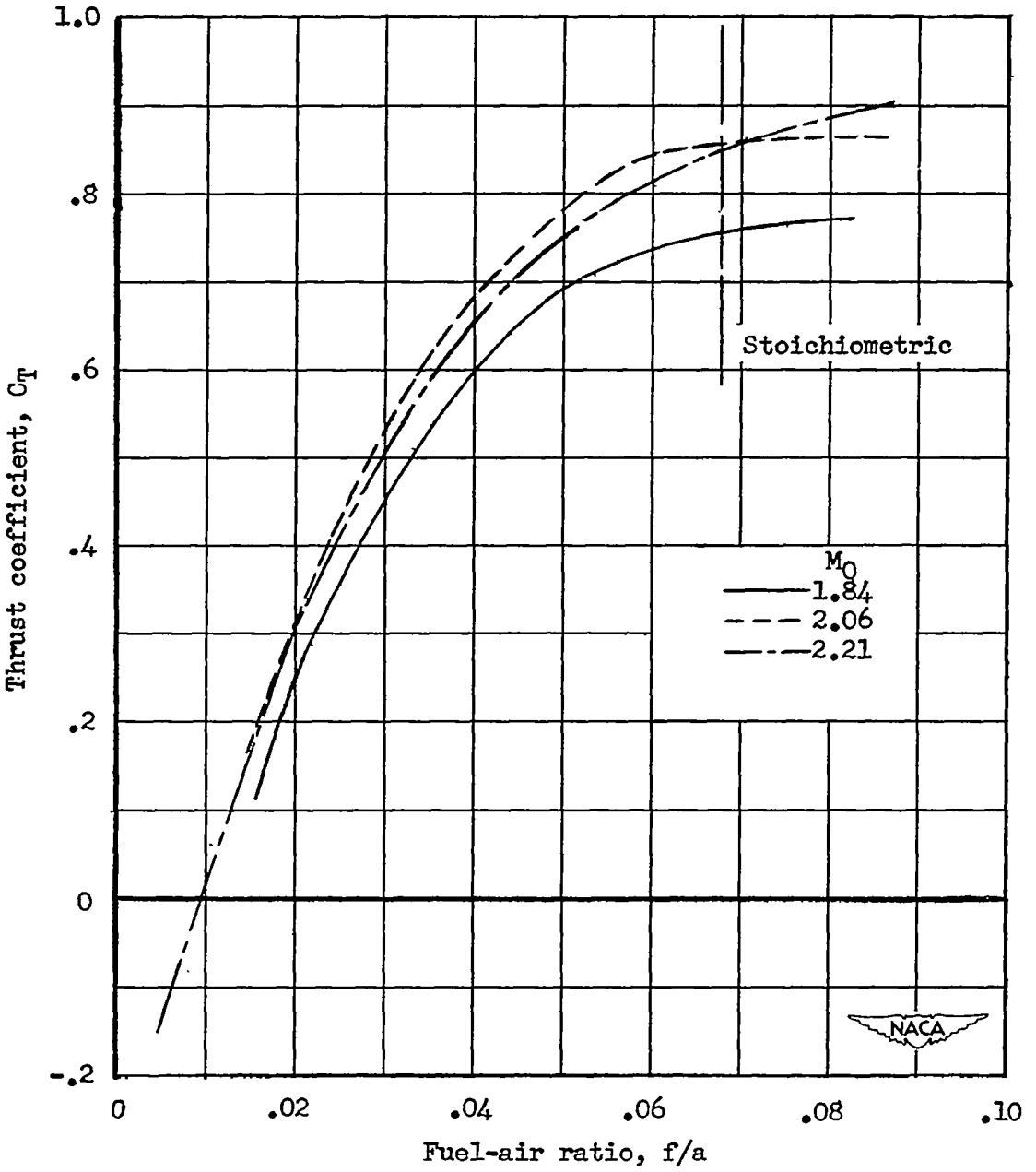

Figure 11.- Thrust characteristics of the ram-jet engine for free-jet Mach numbers of 1.84, 2.06, and 2.21.

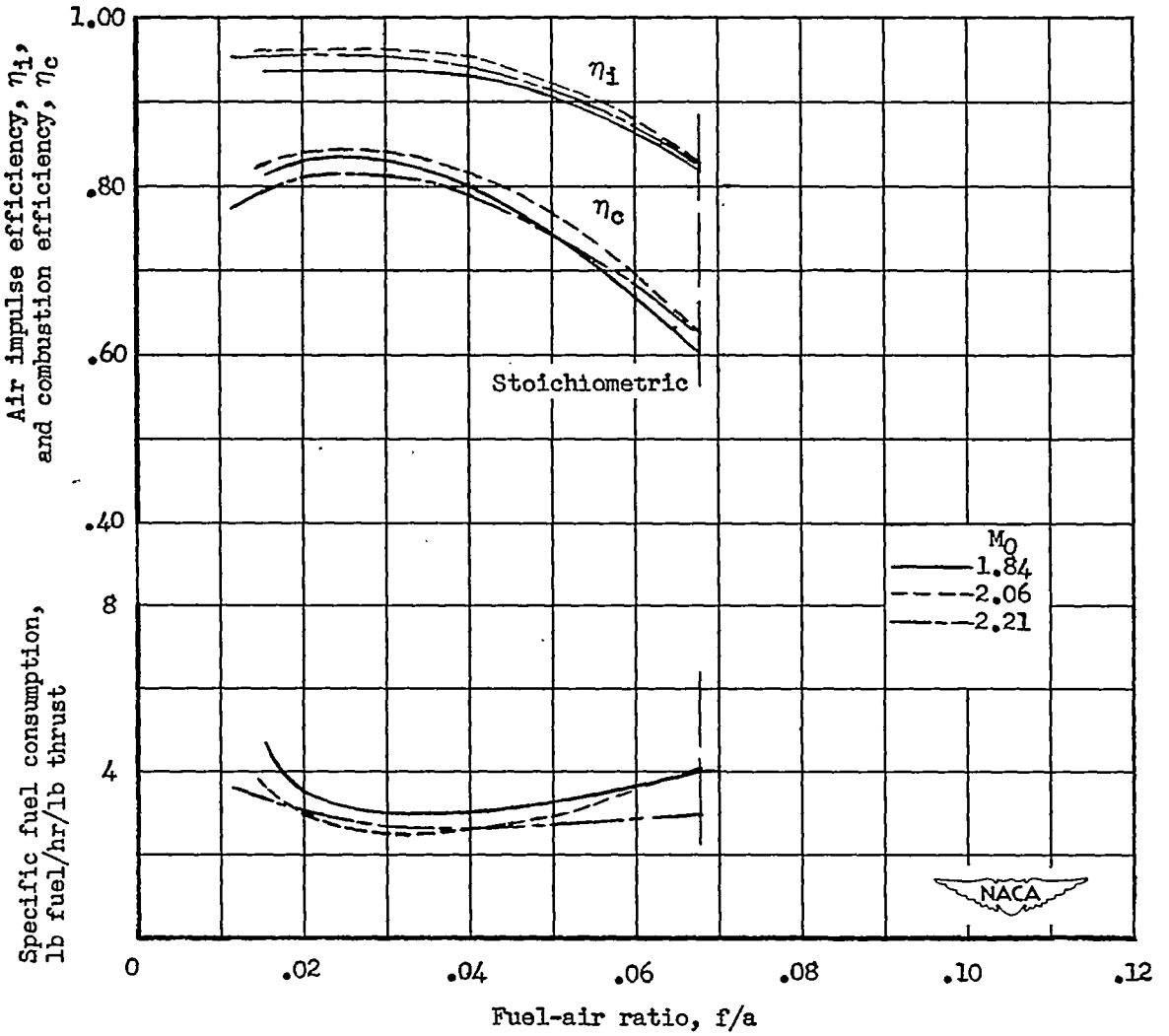

Figure 12.- Air impulse efficiency, combustion efficiency, and the specific fuel consumption of the ram-jet engine as a function of the fuel-air ratio, for free-jet Mach numbers of 1.84, 2.06, and 2.21.

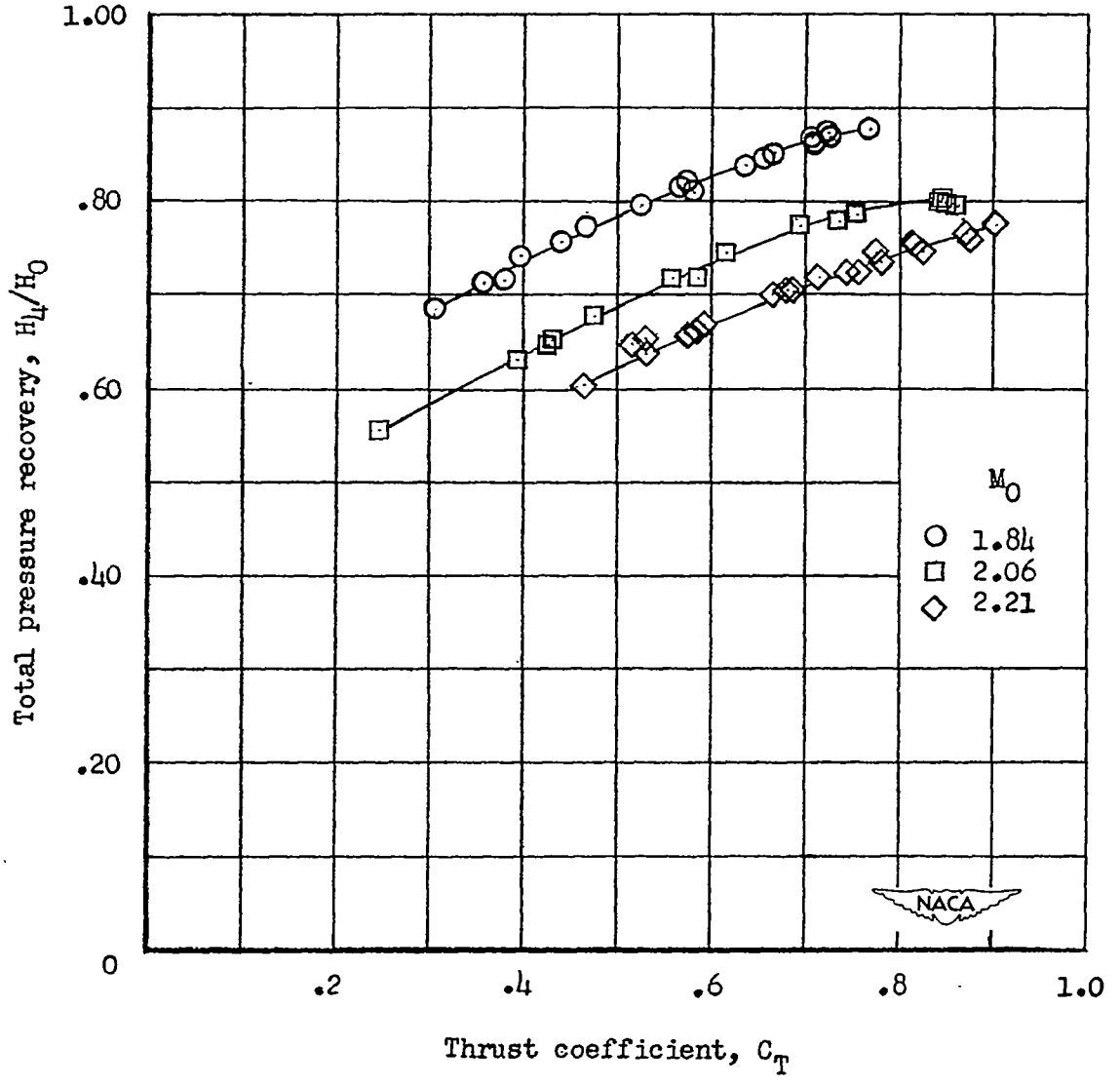

Figure 13.- Total-pressure recovery at station 4 as a function of the thrust coefficient.

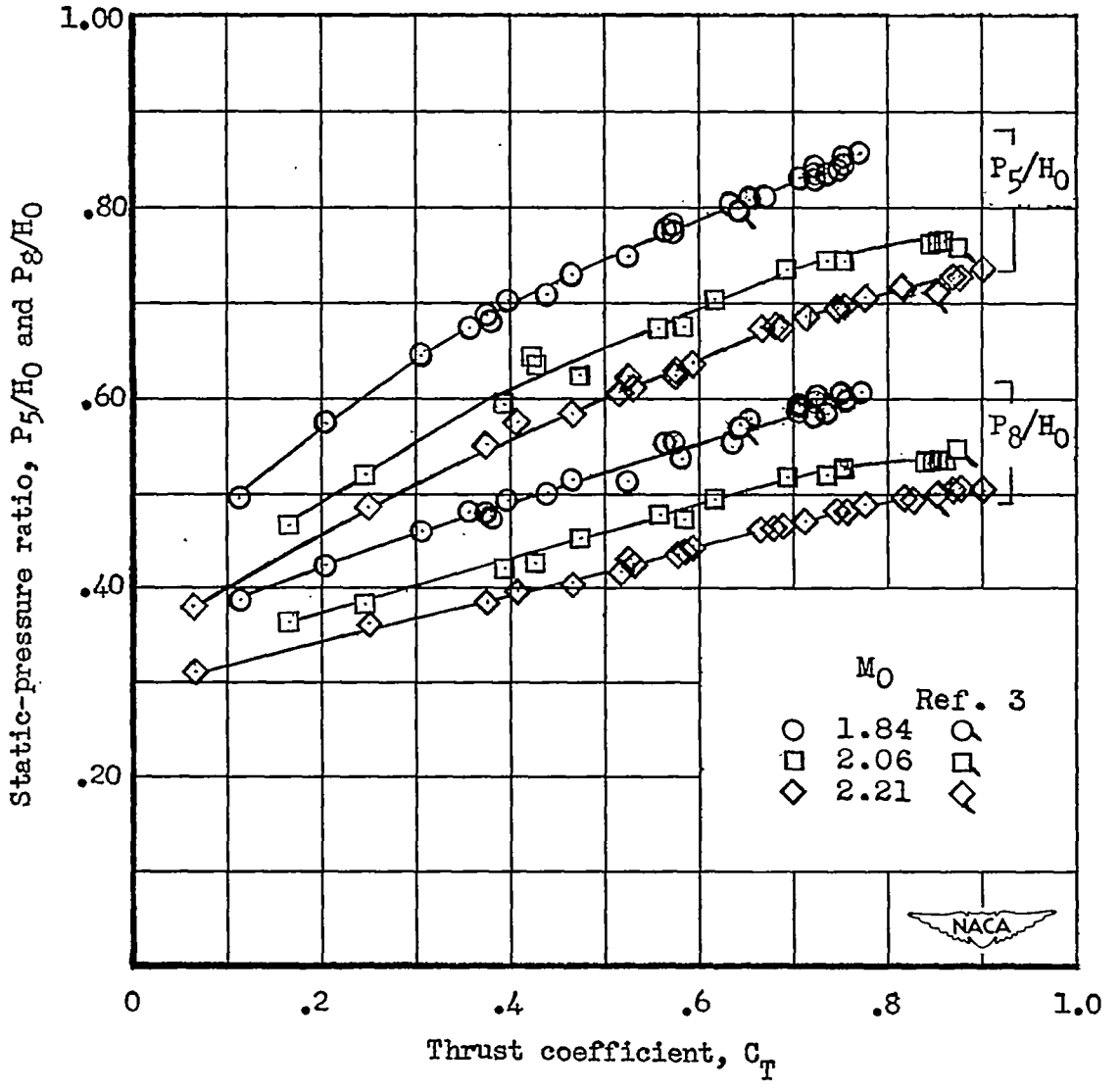

Figure 14.- Static-pressure ratio at station 5 (diffuser exit) and station 8 (combustion chamber exit) as a function of the thrust coefficient.

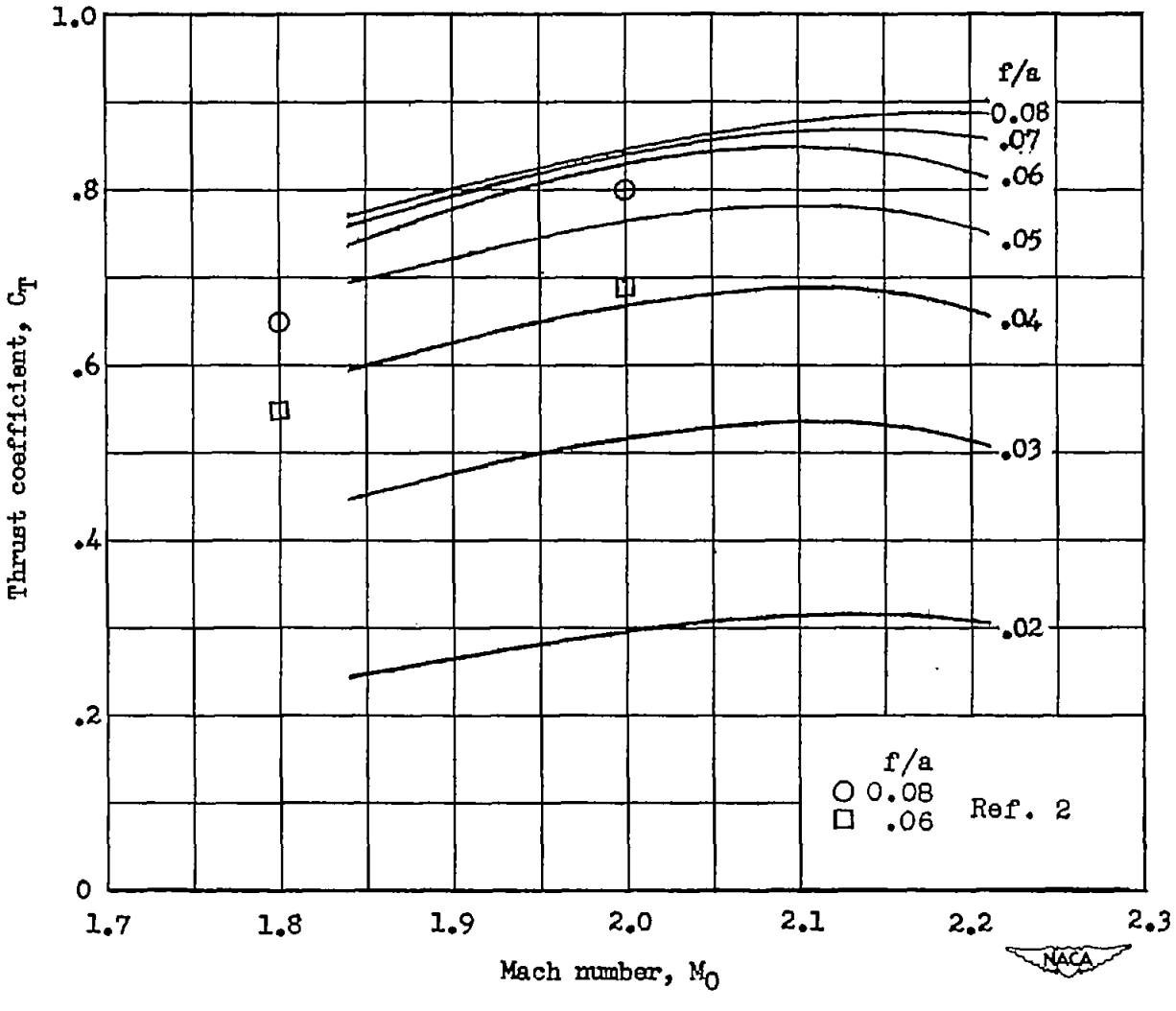

Figure 15.- Thrust coefficient as a function of free-jet Mach number with lines of constant fuel-air ratio.

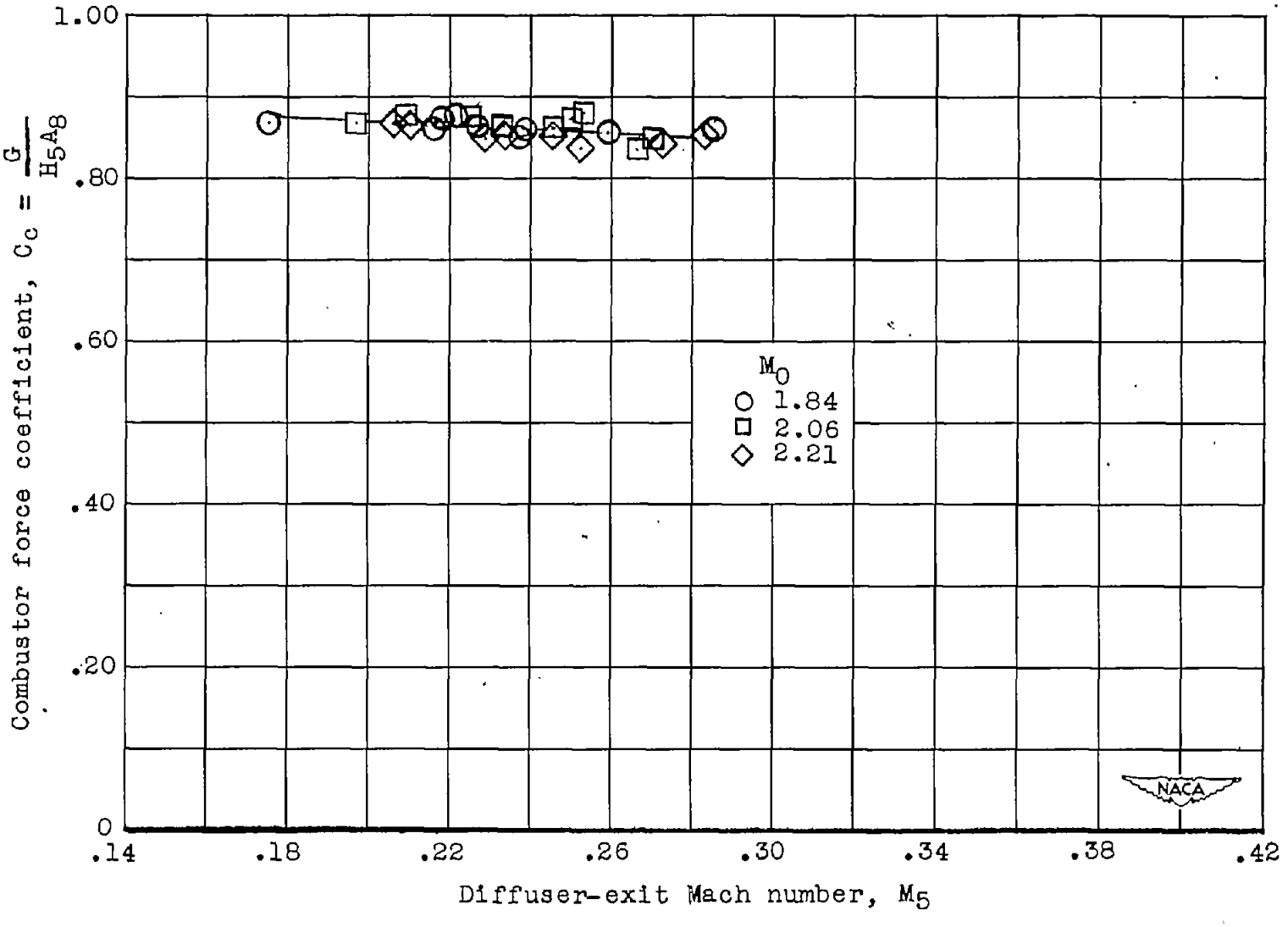

Figure 16.- Combustor force coefficient as a function of the diffuser-exit Mach number for free-jet Mach numbers of 1.84, 2.06, and 2.21.

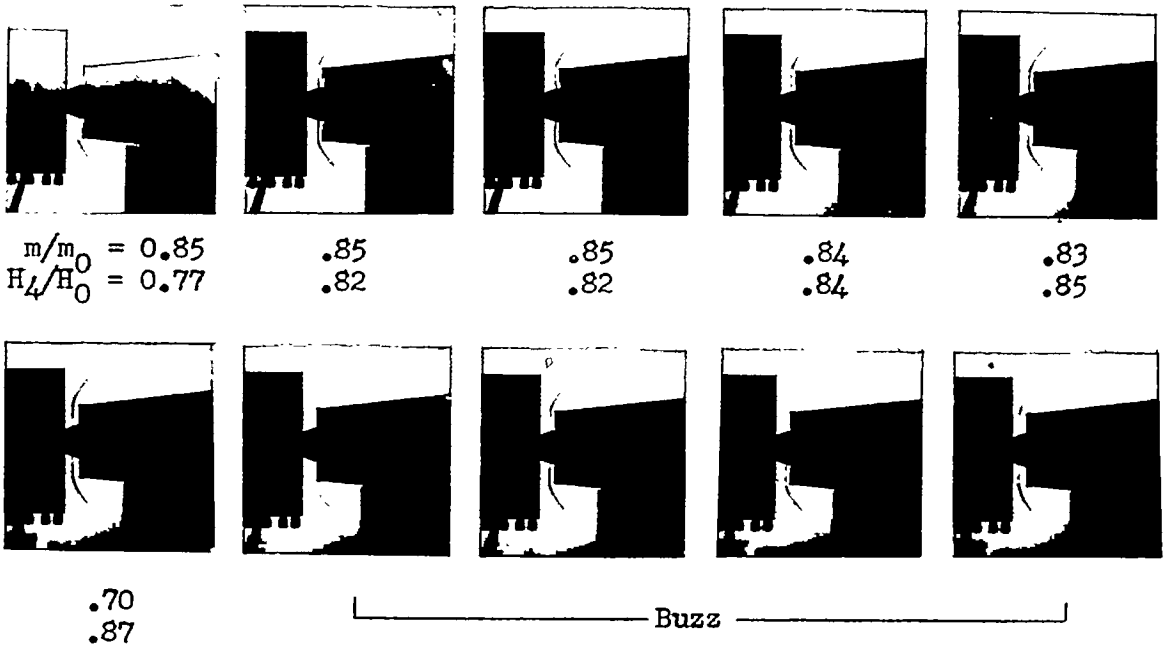

(a) M_0 = 1.84; combustion performance tests.

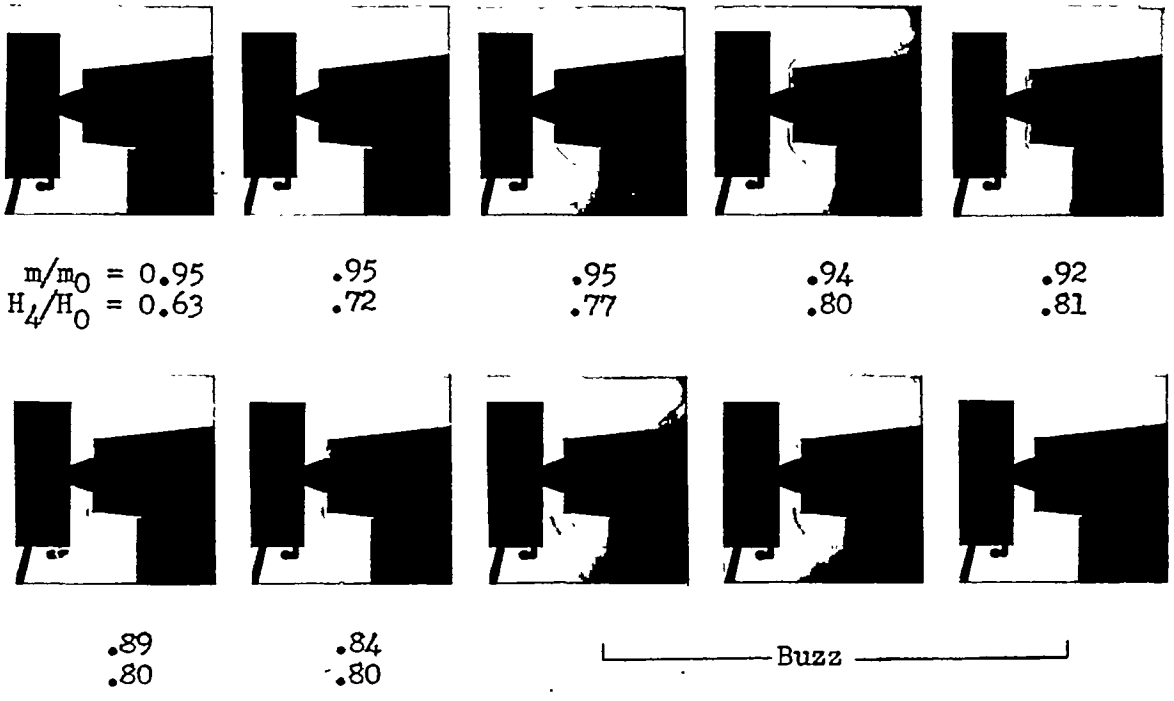

(b) M_0 = 2.06; combustion performance tests. L-80297

Figure 17.- Typical shadowgraph flow patterns of the ram-jet inlet for a range of free-jet Mach numbers. 20° semiangle cone; 0° angle of attack and 0° angle of yaw.

[redacted]

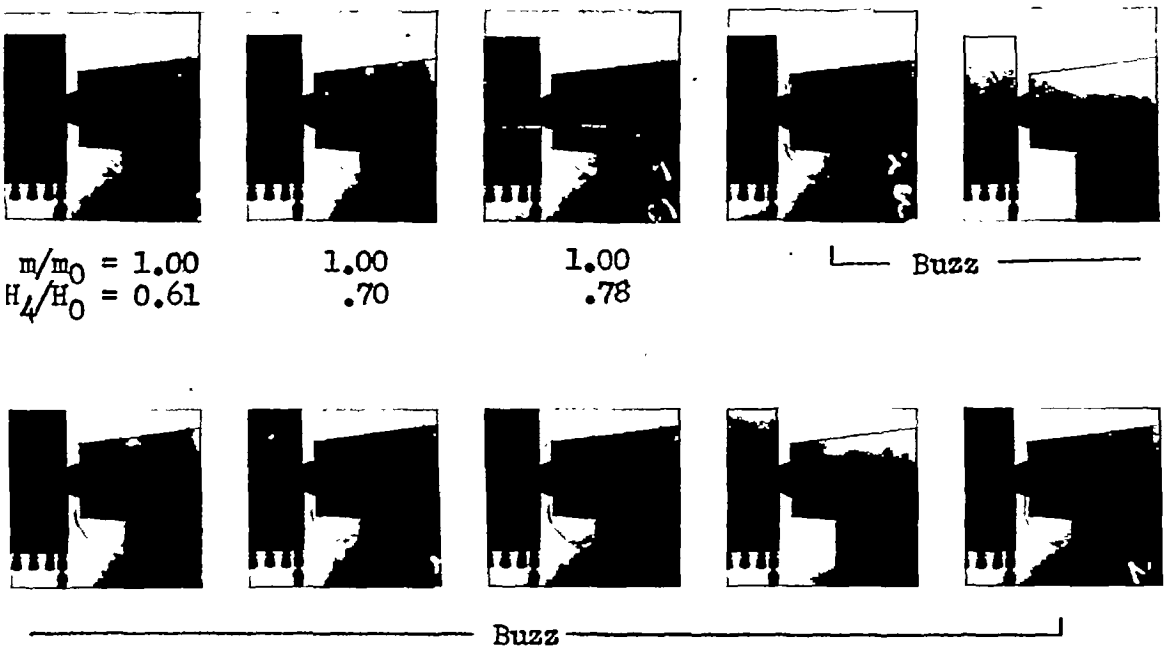

(c) M_0 = 2.21; combustion performance tests.

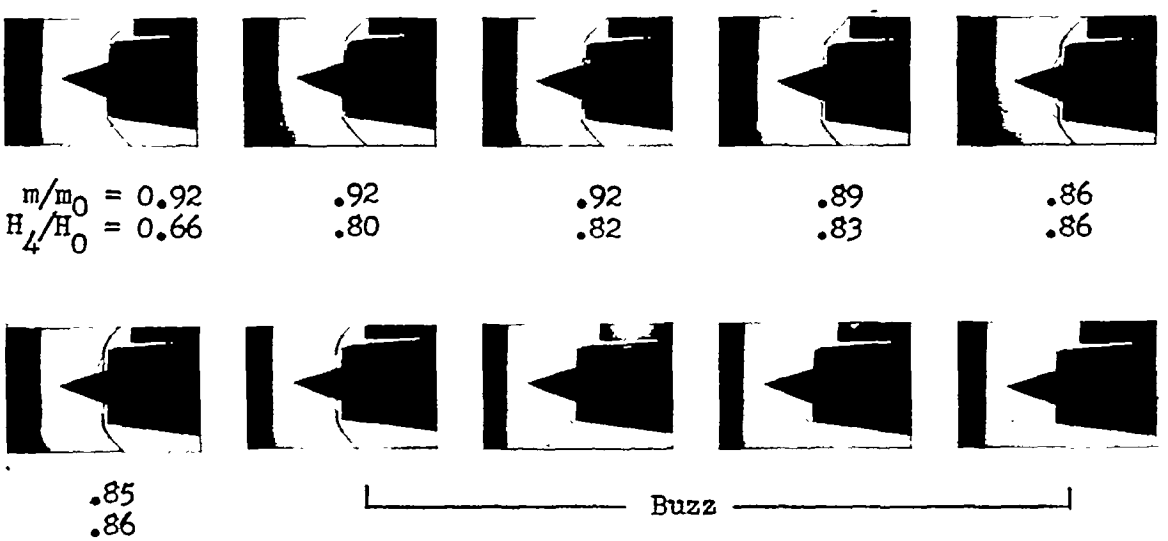

L-80298

(d) M_0 = 2.00; cold-flow tests.

Figure 17.- Continued.

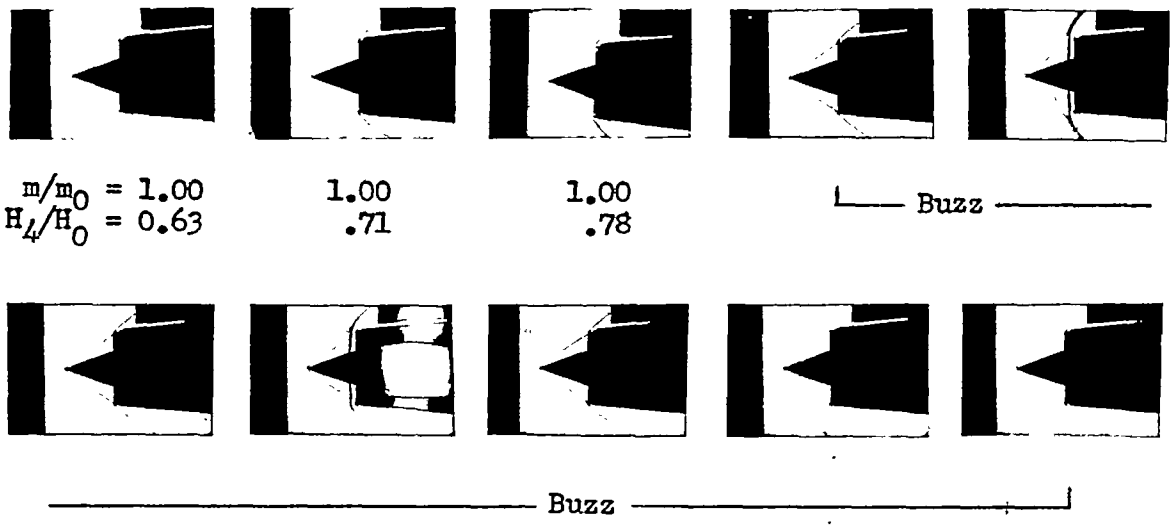

L-80299

(e) M_0 = 2.25; cold-flow tests.

Figure 17.- Concluded.

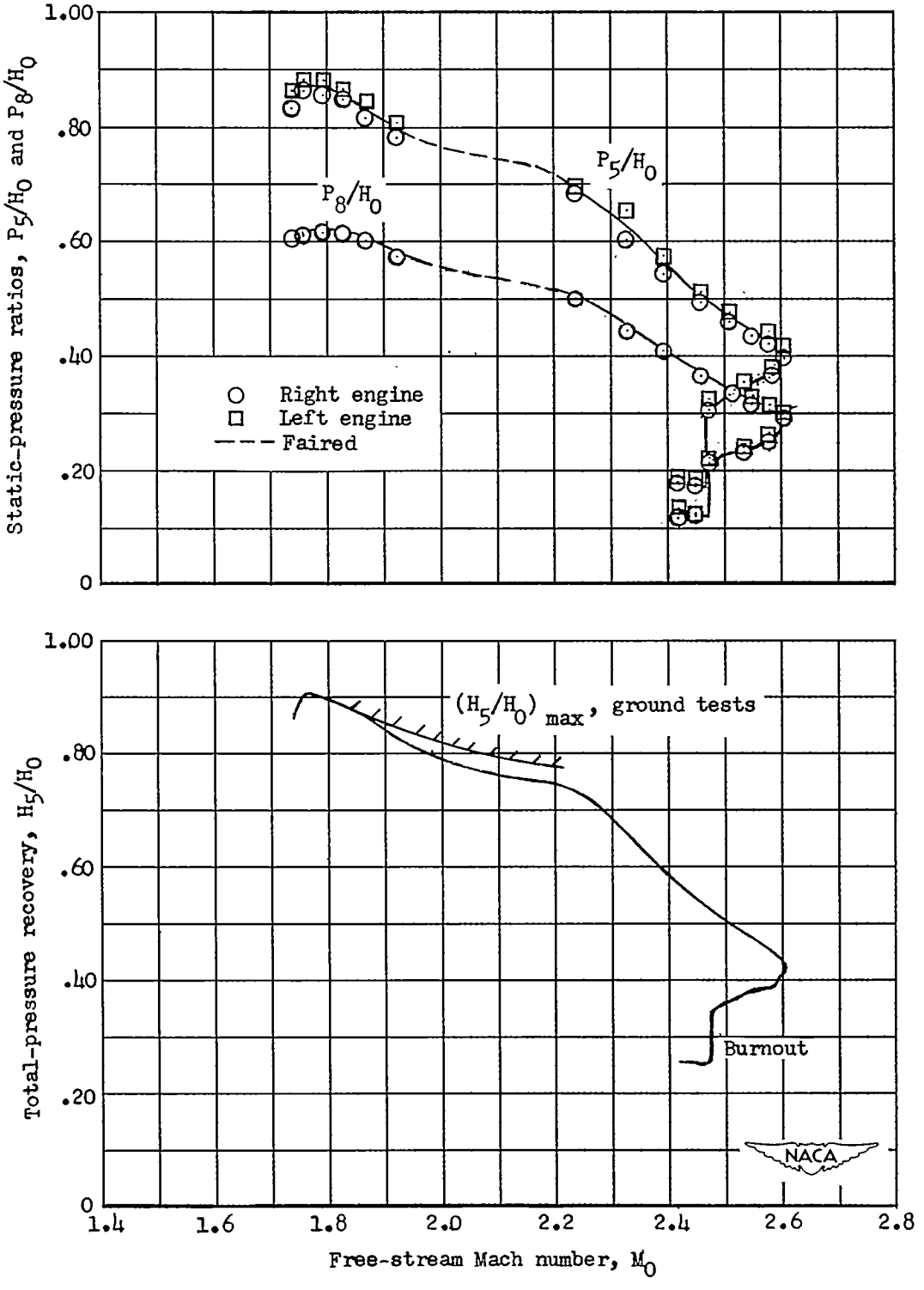

Figure 18.- Diffuser-exit station and combustion-chamber exit station static-pressure ratios and total-pressure recovery as a function of free-stream Mach number for the flight test model.

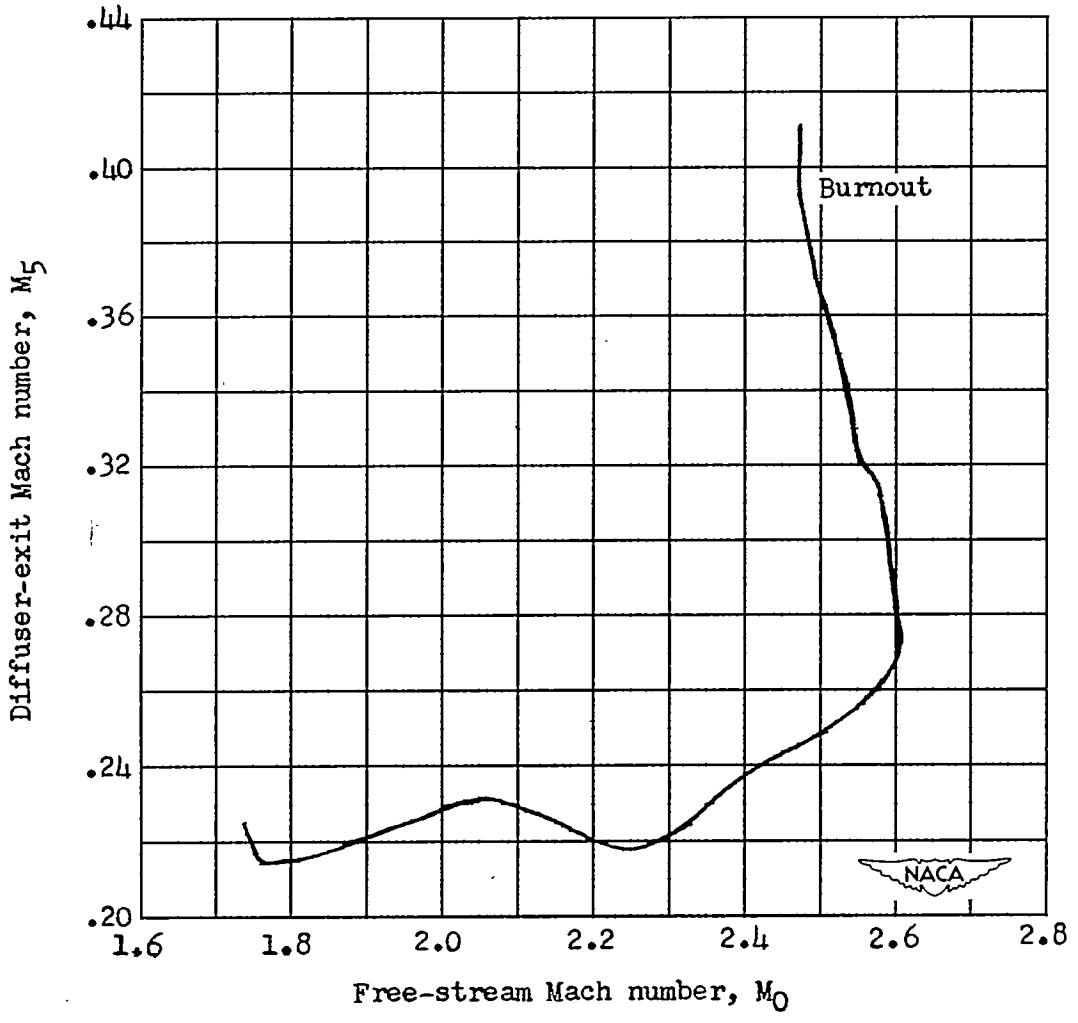

Figure 19.- Diffuser-exit Mach number as a function of free-stream Mach number for the flight test model.

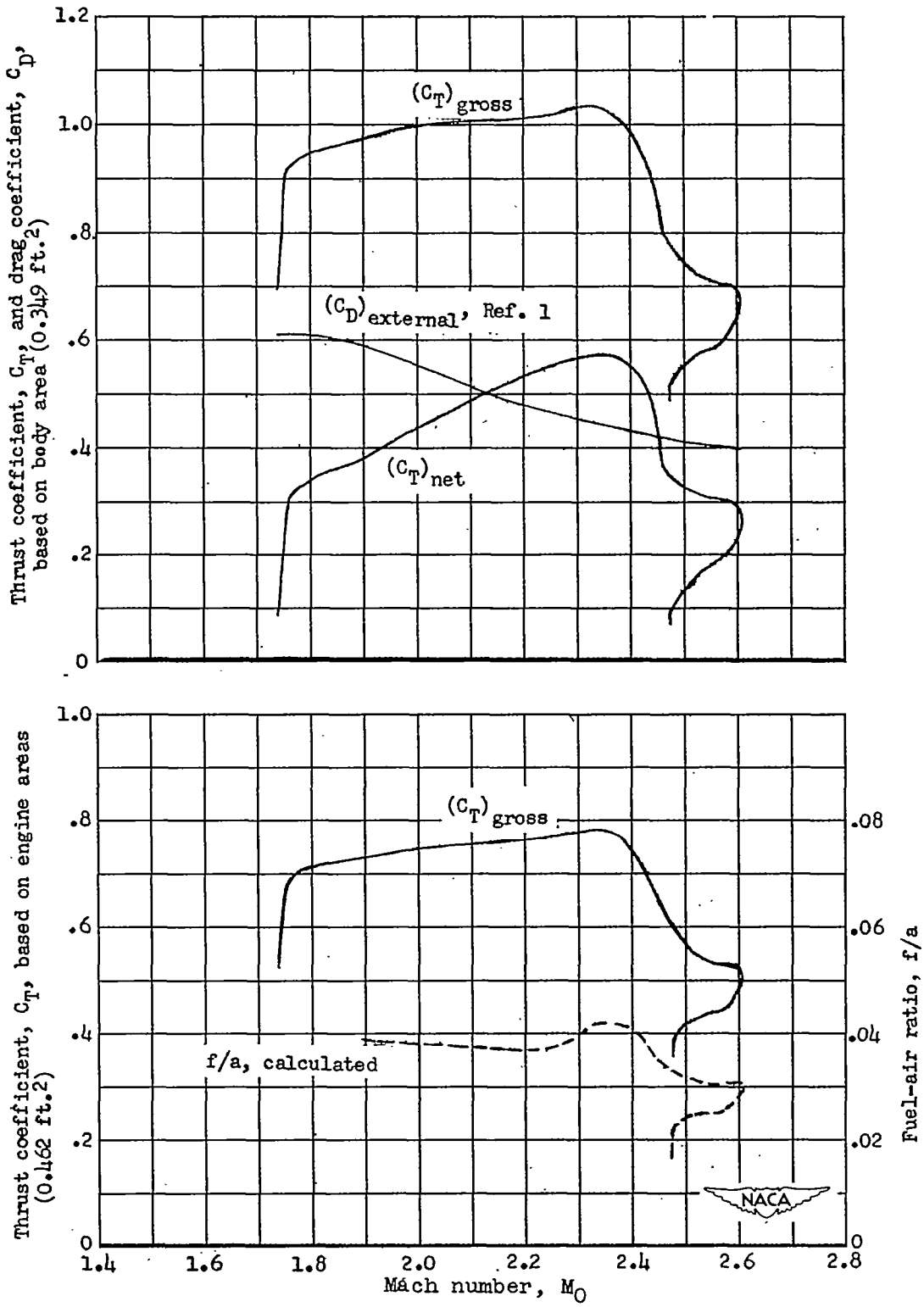

Figure 20.- Thrust coefficient and fuel-air ratio as a function of free-stream Mach number for the flight test model.